August 7th 2019

The quorum sensing transcription factor AphA directly regulates natural competence in *Vibrio cholerae*

James R. J. Haycocks[1], Gemma Z. L. Warren[1], Lucas M. Walker[1], Jennifer L. Chlebek[2], Triana N. Dalia[2], Ankur B. Dalia[2], David C. Grainger*[1]

[1]Institute of Microbiology and Infection, School of Biosciences, University of Birmingham, Edgbaston, Birmingham, B15 2TT, UK.

[2]Department of Biology, Indiana University, Bloomington, IN, USA.

*for correspondence: d.grainger@bham.ac.uk

Tel: +44 (0)121 414 5437

ABSTRACT

Many bacteria use population density to control gene expression via quorum sensing. In *Vibrio cholerae*, quorum sensing coordinates virulence, biofilm formation, and DNA uptake by natural competence. The transcription factors AphA and HapR, expressed at low- and high-cell density respectively, play a key role. In particular, AphA triggers the entire virulence cascade upon host colonisation. In this work we have mapped genome-wide DNA binding by AphA. We show that AphA is versatile, exhibiting distinct modes of DNA binding and promoter regulation. Unexpectedly, whilst HapR is known to induce natural competence, we demonstrate that AphA also intervenes. Most notably, AphA is a direct repressor of *tfoX*, the master activator of competence. Hence, production of AphA markedly suppressed DNA uptake; an effect largely circumvented by ectopic expression of *tfoX*. Our observations suggest dual regulation of competence. At low cell density AphA is a master repressor whilst HapR activates the process at high cell density. Thus, we provide deep mechanistic insight into the role of AphA and highlight how *V. cholerae* utilises this regulator for diverse purposes.

AUTHOR SUMMARY

Cholera remains a devastating diarrhoeal disease responsible for millions of cases, thousands of deaths, and a $3 billion financial burden every year. Although notorious for causing human disease, the microorganism responsible for cholera is predominantly a resident of aquatic environments. Here, the organism survives in densely packed communities on the surfaces of crustaceans. Remarkably, in this situation, the microbe can feast on neighbouring cells and acquire their DNA. This provides a useful food source and an opportunity to obtain new genetic information. In this paper, we have investigated how acquisition of DNA from the local environment is regulated. We show that a "switch" within the microbial cell, known to activate disease processes in the human host, also controls DNA uptake. Our results explain why DNA scavenging only occurs in suitable environments and illustrates how interactions between common regulatory switches affords precise control of microbial behaviours.

INTRODUCTION

Vibrio cholerae colonises two distinct habitats; the human intestine and aquatic ecosystems [1]. In the aquatic niche, the microbe forms biofilms on chitinous surfaces [2,3]. This induces expression of the gene regulatory protein TfoX [4-6]. Natural competence, the ability to acquire exogenous DNA from the environment, is triggered as a result [7-9]. Specifically, TfoX stimulates production of a type IV pilus that extends to bind, and retracts to internalise, exogenous DNA [10-13]. Genes encoding important cell envelope factors ComEA and ComEC, are also TfoX regulated [14]. Biofilms disperse upon entering the human gut [1,15]. This triggers the expression of virulence factors. Notably, the toxin co-regulated pilus (TCP) and cholera toxin (CT) are produced [16]. These factors are encoded by the *tcpPH* and *ctxAB* operons respectively.

Quorum sensing detects changes in bacterial population density reported by auto-inducer molecules [17]. This information is used to modify patterns of gene expression [18]. For example, CqsS is a membrane bound sensor kinase that detects cholera auto-inducer 1 (CAI-1) [19]. When kin are scarce, and CAI-1 levels low, CqsS triggers a regulatory cascade, which cumulates in expression of five quorum regulatory RNAs [20]. These RNA molecules activate translation of AphA, a PadR family transcription factor with an N-terminal winged helix-turn-helix DNA binding motif [20-22]. In turn, AphA activates expression of *tcpPH* [23]. This event ignites the entire virulence gene expression programme [16]. Surprisingly, given the central role of AphA, the regulator is poorly understood. For instance, transcriptome analysis found just 6 operons controlled by AphA in *V. cholerae*, 5 of these indirectly [24]. Conversely, in closely related *Vibrio harveyi*, perturbation of *aphA* impacted transcription of hundreds of genes [22,25]. The DNA binding properties of AphA are also incompletely defined. Three studies have proposed a DNA consensus motif that binds AphA [24,26,27]. Though there are similarities, the sequence differs in each report. Thus, whilst a key factor in *V. cholerae*, the extent and mechanistic basis of regulation by AphA is not understood.

In this study, we sought to better understand the DNA binding and gene regulatory properties of AphA in *V. cholerae*. Using chromatin immunoprecipitation (ChIP) and DNA sequencing (ChIP-seq) we mapped genome-wide DNA binding by AphA. This revealed a palindromic consensus for AphA recognition. Interactions can involve single targets or co-operative AphA binding to adjacent sites. Though discovered as an activator of pathogenicity, AphA mainly targets genes related to cell surface physiology, including a subset required for natural competence. These target genes encode components of the type IV pilus, the competence regulator TfoX, and the quorum sensing factor CqsS. The mechanistic details vary but, at each locus, AphA acts as a transcriptional repressor. We conclude that AphA plays a key role by coupling natural competence to population density in *V. cholerae*.

RESULTS

Genome-wide distribution of AphA in Vibrio cholerae

To identify genes targeted by AphA we used ChIP-seq. The data are illustrated in Figure 1a. In each plot, genes are shown as blue lines (outer two tracks) and the binding profile of AphA is in teal (inner track). We identified 49 binding peaks for AphA. The peaks were not distributed evenly; 27 % were located within a 0.5 Mbp section of chromosome II accounting for only 12 % of the total genome (Figure 1a). To assess data validity, we determined the position of each peak with respect to the nearest gene start codon (Figure 1b). As expected, AphA peak positions cluster at the 5' ends of genes. Counterintuitively, this was true even though two thirds of peaks were located within coding sequences (Figure 1b, inset). This apparent contradiction arises because many peaks close to start codons are within adjacent genes. Examples of such peaks are shown in Figure 1c. Next, we extracted DNA motifs from the peak sequences using MEME. A single significant ($E = 2.2^{-7}$) DNA motif was found (Figure

1d). This palindromic sequence (5'-ATGCAA-N_4-TTGCAT-3') likely represents the preferred AphA binding target. We determined the distance between each occurrence of the motif and the centre of the ChIP-seq peak. As expected, the motif is biased to the centre of the ChIP-seq signal (Figure 1e, teal bars). The MEME analysis also identified motifs that were not statistically significant (data not shown). These sequences were randomly distributed with respect to AphA peak centres. An example is shown as a control in Figure 1e (grey bars). The position of each peak, adjacent genes, and AphA binding motif is listed in Table 1. The distribution of functions associated with AphA targeted genes is shown in Figure 1f. We found that AphA primarily targeted genes for other regulatory proteins and components of the cell envelope. Most interestingly, AphA bound at three loci adjacent to genes known to influence DNA uptake by natural competence (Table 1). Briefly, these loci are the intergenic region between VC0857 and VC0858, the VC1153 (*tfoX*) promoter region, and the regulatory DNA for VCA0522 (*cqsS*). Importantly, purified AphA also recognised these targets specifically *in vitro* (Figure S1). Hence, we next sought to understand the role of AphA at each locus.

AphA binds a single site at the intergenic region between VC0857 and VC0858

The genes VC0857 and VC0858 encode homologues of the minor pilins *fimT* and *pilE*. Such proteins are hypothesised to initiate assembly of the DNA uptake pilus and reside at the tip of the pilus fibre [28,29]. Indeed, the VC0858 and VC0857 gene products contribute to pilus-DNA interactions, which occur specifically at the pilus tip [13]. The ChIP-seq data for AphA binding at the intergenic region between VC0857 and VC0858 is shown in Figure 2a. The sequence of the intergenic region is shown in Figure 2b. To precisely identify the AphA binding site we used DNAse I footprinting (Figure 2c). The data show that AphA binding protects a 25 bp region of DNA from digestion by DNAse I. The footprint coincides with a DNA sequence (ATGAAT-N_4-TTGCAT) that matches our motif for AphA binding at 10 of 12 positions (boxed in Figure 2b). The sequence also coincides precisely with the centre of the ChIP-seq peak (asterisk in Figure 2b).

AphA prevents binding of RNA polymerase to the VC0857/VC0858 intergenic region and inhibits transcription

The transcription start sites (+1) for VC0857 and VC0858 are denoted by bent arrows in Figure 2b [30]. The corresponding promoter DNA elements are underlined. The AphA binding site overlaps the transcription start site for VC0858 and the promoter -35 element for VC0857 (Figure 2b). We reasoned that binding of AphA would be incompatible with binding of RNA polymerase to the regulatory region. To test this, we used electrophoretic mobility shift assays (EMSAs). The data show that AphA retarded migration of the regulatory DNA fragment (Figure 2d, compare lanes 1 and 2). A substantial change in electrophoretic mobility was evident when RNA polymerase was added instead of AphA (Figure 2d, compare lanes 1 to 3). Inclusion of AphA in incubations with RNA polymerase resulted in DNA migration similar to that with AphA alone (compare lanes 2 and 4). Hence, AphA appears to interfere with the binding of RNA polymerase. To measure the impact of AphA on promoter activity we used *in*

vitro transcription assays. Hence, the DNA sequence in Figure 2b was cloned, in either the forward or reverse orientation, upstream of the λ*oop* terminator in plasmid pSR. Transcripts generated from the cloned DNA can be quantified after electrophoresis. The 108 nt RNAI transcript derives from the pSR replication origin and serves as an internal control. We were unable to detect transcripts from the VC0858 promoter (data not shown). Conversely, a transcript of the expected size was generated by the VC0857 promoter (Figure 2e, lane 1). Addition of AphA abolished production of the transcript but not synthesis of the RNAI control (Figure 2e, lane 2). We also fused the regulatory fragment to *lacZ* in plasmid pRW50T. Next, *V. cholerae* strains with or without *aphA* were transformed using the plasmid derivatives. As with our *in vitro* analysis, we detected no transcription from the *VC0858* promoter (data not shown). Hence, we can infer little about potential regulation of *VC0858* by AphA. However, *lacZ* expression was driven by the VC0857 promoter. Recall that AphA is active at low bacterial population densities. Hence, we measured β-galactosidase activity in different phases of growth. The results are shown in Figure 2f. In wild type cells, VC0857 promoter activity increased rapidly once the culture reached the optical density of ~0.8. (Figure 2f, solid line). In cells lacking AphA, the promoter was active at a markedly lower population density (Figure 2f, dashed line). We conclude that AphA is a repressor of VC0857 expression and exerts this effect by occluding the binding site for RNA polymerase (Figure 2g). Interestingly, whilst VC0857 is activated by quorum sensing auto-inducer molecules, which prevent AphA expression, VC0858 is unresponsive (Table 1).

AphA co-operatively binds two adjacent sites at the tfoX *promoter*

We next turned our attention to the regulatory region upstream of the *tfoX* gene. Briefly, TfoX is a master activator of all genes required for natural competence [11]. Hence, the decision to express *tfoX* is a major checkpoint. The ChIP-seq data for AphA binding upstream of *tfoX* is shown in Figure 3a. The corresponding gene regulatory region is shown in Figure 3b. The centre of the AphA binding peak is again denoted by an asterisk. Note that expression of *tfoX* is almost completely dependent on CRP binding to a site (orange in Figure 3b) centred 83.5 bp upstream of the *tfoX* transcription start site (bent arrow in Figure 3b) [31]. We first used DNAse I footprinting to pinpoint AphA binding to the *tfoX* regulatory region (Figure S2a, lanes 2-4). The AphA footprint occurs between promoter positions -73 and -110. It is important to note that the upstream boundary of the footprint is demarked by a subtle change in the pattern of DNAse I digestion; protection of the base at position -109 and DNAse I hypersensitivity at position -110. This transition is marked by the teal arrow adjacent to lane 4 in Figure S2a. Since the AphA footprint extends over 37 bp it likely represents AphA binding two adjacent sites. The proposed sites are labelled AphA I and AphA II in Figure 3b. The sequences coincide precisely with the centre of the ChIP-seq peak for AphA binding. Sites AphA I (5'-CAACAA-N_4-TTGACG-3') and AphA II (5'-GTGATA-N_4-TCTCAT-3') match the consensus for AphA binding at 6/12 and 7/12 positions respectively. Hence, these seem comparatively poor binding targets. To understand how AphA recognises these sequences we mutated site AphA I or AphA II (red in Figure 3b). We then used

DNAse I footprinting to investigate the consequences. Mutations in the upstream AphA I site changed only the upstream half of the large AphA footprint (Figure S2a, lanes 5-7). Hence, the hypersensitive band at position -110 did not appear. We also observed poor protection of a band at position -100 (see triangle to the right of lane 7 in Figure S2a). Mutations in the downstream AphA II site had pronounced consequences. First, the mutations changed the overall pattern of DNAse I sensitivity (compare lanes 2 and 8 in Figure S2a). Second, the mutations rendered AphA unable to bind to either site I or site II (Figure S2a, lanes 8-10). We conclude that AphA binds its two adjacent sites at the *tfoX* regulatory region co-operatively. Hence, mutations in site AphA II, a closer match to the consensus, abolish recognition of both targets.

AphA and CRP compete for overlapping binding sites upstream of the tfoX promoter

Strikingly, the region of the *tfoX* promoter bound by AphA overlaps the binding site for CRP (orange in Figure 3b). We reasoned that AphA and CRP may compete for binding. To test this, we further utilised DNAse I footprinting (Figure 3c). Fortuitously, although CRP and AphA bound similar locations, the footprints produced were easily distinguished. Thus, CRP binding resulted in DNAse I hypersensitivity at positions -83 and -92 upstream of the *tfoX* promoter (Figure 3c, lane 3). As already noted, AphA binding protected the DNA and induced DNAse I hypersensitivity at promoter position -110 (Figure 3c, lane 4). The sites of DNAse I hypersensitivity due to CRP and AphA binding respectively are shown by orange and teal triangles to the right of Figure 3c. Next, we added increasing concentrations of AphA to incubations containing the *tfoX* promoter DNA fragment and CRP (Figure 3c, lanes 5-9). As the concentration of AphA increased so did the occurrence of DNAse I hypersensitivity at position -110. Concomitantly, DNAse I hypersensitivity at positions -83 and -92, due to CRP binding, was reduced. In parallel experiments we measured binding of AphA and/or CRP to the *tfoX* promoter region using EMSAs (Figure 3d). Addition of AphA or CRP to incubations altered migration of the *tfoX* promoter DNA fragment during electrophoresis. Importantly, the degree to which migration altered was different for each protein (compare lanes 1-3 in Figure 3d). This is most likely because CRP bends the DNA by 90° whilst AphA has little effect [21,32,33]. Addition of AphA reduced the abundance of complexes due to CRP and increased the abundance of the complexes due to AphA (Figure 3d, lane 4). Thus, AphA and CRP compete for binding the same section of the *tfoX* gene regulatory region. Note that AphA could outcompete CRP even if the latter was present at higher concentrations (Figure 3d). We conclude that AphA is likely an anti-activator of *tfoX* expression (i.e. the repressor targets the activator rather than RNA polymerase directly).

AphA prevents activation of tfoX *expression mediated by CRP*

To investigate the effects of AphA and CRP on *tfoX* promoter activity we used *in vitro* transcription. As expected, activation of *tfoX* transcription by CRP was evident (Figure 3e, lanes 1-4). Addition of AphA abolished activation by CRP (lanes 5-8). To investigate repression *in vivo* we utilised the *lacZ* reporter plasmid described above. In wild type cells *tfoX* promoter activity increased in line with culture

optical density (Figure 3f, solid line). The pattern of *tfoX* promoter activity was different in the absence of AphA (Figure 3f, dashed line). In particular, β-galactosidase activity increased to 5-fold higher levels in the early- to mid-exponential phase of growth. Our model for regulation of *tfoX* promoter activity by AphA and CRP is shown in Figure 3g.

AphA and CRP bind the cqsS *regulatory region in unison*

The final AphA target selected for characterisation was adjacent to *cqsS*. The CqsS protein is at the top of the regulatory cascade triggered by the quorum sensing auto-inducer molecule CAI-1 [20]. At high population densities the cascade prevents expression of downstream genes including *tfoX* and *aphA*. The ChIP-seq signal for AphA binding upstream of *cqsS* is shown in Figure 4a and the sequence of the regulatory region is shown in Figure 4b. We again used DNAse I fooprinting to dissect binding of AphA (Figure S2b). The footprint due to AphA was 37 bp in length (Figure S2b, lanes 2-4). This was indicative of two adjacent AphA sites (labelled I and II in Figure 4b). Mutations made in each site are shown in Figure 4b (red text) and footprints done using the mutated DNA fragments are in Figure S2b. Mutations in the upstream AphA I site completely abolished binding of AphA to both targets (Figure S2b, lanes 5-7) whilst mutations in the downstream AphA II site only prevented binding to the second occurrence of the motif (Figure S2b, lanes 8-10). Hence, we again conclude that AphA recognises two sites co-operatively at the *cqsS* promoter region. Importantly, the two sites overlap precisely with the DNAse I footprint and the centre of the ChIP-seq peak (asterisk in Figure 4b). The AphA sites also overlap the *cqsS* transcription start site (bent arrow in Figure 4b) [30]. We noticed that the *cqsS* regulatory region contained an 8/10 match to the consensus sequence for CRP binding (orange in Figure 4b) centred 41.5 bp upstream of the *cqsS* promoter. This is intriguing because CRP enhances expression of CqsA, which synthesises CAI-1 detected by CqsS [34]. Hence, we sought to understand if CRP bound this site. The results of DNAse I footprinting experiments are shown in Figure 4c. As expected, CRP (lane 3) and AphA (lane 4) produced footprints at their respective target sites. Addition of AphA to incubations containing CRP resulted in footprinting of both the AphA and CRP targets (lanes 5-7). Similar results were obtained in parallel EMSAs (Figure 4d). Hence, AphA (lane 2) and CRP (lane 3) both individually bound to the *cqsS* DNA fragment. A super-shifted complex was observed when the proteins were added in unison (lane 4).

AphA and CRP oppositely regulate the cqsS *promoter*

To understand the effects of AphA and CRP on *cqsS* promoter activity we first used *in vitro* transcription assays (Figure 4e). A transcript was only generated from the *cqsS* promoter in the presence of CRP, albeit at low levels (lanes 1 and 2). In the presence of CRP and AphA this transcript was undetectable (lanes 4-6). Because the *cqsS* promoter was poorly active in our *in vitro* transcription analysis we also used $KMnO_4$ footprinting. This detects DNA opening by RNA polymerase at promoter -10 elements during transcription initiation. The results are shown in Figure 4f; the appearance of bands is indicative of DNA melting. Such bands were only observed in the presence of both CRP and RNA polymerase

(lane 6). Addition of AphA to incubations with CRP and RNA polymerase prevented promoter unwinding (lanes 7-9). The low level transcription detected *in vitro* (Figure 4e) was recapitulated using a *cqsS*::*lacZ* fusion *in vivo* (Figure 4g). Hence, only 120 Miller units were detected for experiments with the *cqsS* promoter; 20-fold lower than equivalent experiments with the *tfoX* promoter (compare Figures 3f and 4g). Surprisingly, β-galactosidase activity in lysates of wild type and Δ*aphA* cells were similar (compare solid and dashed lines in Figure 4g). We conclude that AphA is likely to be a repressor of the *cqsS* promoter. However, specific conditions may be required to detect such repression *in vivo* (Figure 4h). We note that addition of quorum sensing auto-inducer molecules, which block production of AphA, activate *cqsS* expression (Table 1).

Deleting aphA *enhances natural competence at low cell density*

Whether *V. cholerae* cells act individually or as a group is coupled to population density by the regulator LuxO [20,35]. Consequently, the LuxO^{D47E} substitution, which is phosphomimetic, locks cells in a low density state. This mutation is frequently exploited to study behaviours specific to this mode of life [22,36]. Our data suggest that AphA represses the regulatory cascade triggering natural competence at low population density. To test this, we introduced *luxO*^{D47E} into *V. cholerae* E7946 and a derivative lacking *aphA*. It was also necessary to delete *dns*; the gene encodes an endonuclease expressed at low cell density to degrade any DNA obtained by natural transformation [37]. We then measured the frequency of transformation by natural competence for each strain. The result of the experiment is shown in Figure 5a (speckled bars). As expected, the E7946 strain encoding LuxO^{D47E} was poorly transformable. Consistent with our model, deletion of *aphA* triggered a ~1,500 fold increase in transformation frequency. Hence, AphA is a repressor of natural competence.

Expression of aphA *reduces natural competence at high cell density*

We next examined transformation of E7946, and the derivative lacking *aphA*, in the context of the wild type *luxO* allele. These strains transition to a high cell density, and become naturally competent, upon colonisation of chitinous surfaces. In this scenario, wild type E7946 were transformed efficiently. However, because *aphA* is not expressed at high cell density, deleting the gene had no effect (Figure5a, open bars). We reasoned that differences in transformation frequency would be observed if *aphA* was expressed ectopically. To achieve this, *V. cholerae* strain E7946 was transformed with plasmid pAMCF*aphA* that encodes the C-terminally 3xFLAG tagged AphA used in our ChIP-seq experiments. Importantly, the level of AphA generated from this plasmid precisely matches that of chromosomally encoded AphA (Figure S3). As a control, we utilised plasmid pAMNF*aphA* encoding N-terminally 3xFLAG tagged AphA, which cannot bind DNA (see control ChIP-seq data). Expression of the active C-terminally tagged AphA reduced DNA uptake by ~1,300-fold. Comparatively, N-terminally tagged AphA had little effect (compare open and black bars in Figure 5a).

Uncoupling TfoX expression from AphA regulation largely restores natural transformation

We next sought to understand which of the AphA regulatory events described above (Figures 2-4) resulted in the loss of competence phenotype due to constitutive AphA production. First, we focused our attention on *tfoX* repression by AphA. If responsible for reduced competence, natural transformation should be restored by uncoupling *tfoX* expression from AphA regulation. To do this we replaced the native *tfoX* promoter with the IPTG inducible *tac* promoter (P_{tac}-*tfoX*) in strains containing pAMCF*aphA* or pAMNF*aphA*. Expression of *tfoX* almost completely abolished the effect of constitutive AphA production on natural transformation (compare black and grey bars in Figure 5a). We conclude that AphA mediated *tfoX* repression is the primary cause of reduced natural transformation in our experiments.

Constitutive expression of AphA does not impact pilus production

Our focus turned to the residual 6-fold effect of AphA observed in the presence of ectopic *tfoX* expression (see the difference between grey bars in Figure 5a). We reasoned that attenuated pilus activity, due to repression of VC0857 by AphA, might be responsible. To monitor pilus production, we utilised *V. cholerae* encoding $PilA^{S67C}$ [13]. The cysteine substitution facilitates *in vivo* labelling of PilA with the fluorescent dye AF488-mal. Since PilA is a major component of the DNA uptake apparatus, this allows visualisation of pili in live cells. Recall that TfoX is an activator of VC0857 [11]. To avoid indirect effects of AphA, mediated by repression of *tfoX*, we again utilised P_{tac}-*tfoX*. The supplementary movies S1 and S2, and the representative images in Figure 5b, show dynamic pilus events (white arrows). We compared cells expressing the non-functional N-terminally tagged AphA or the active C-terminally tagged derivative. A quantification of the data is shown in Figure 5c; there was no significant difference between strains ($P = 0.06$). We conclude that repression of VC0857 by AphA has little impact on DNA uptake in the conditions of our assay.

Deleting luxO does not bypass inhibition of natural competence by AphA

To determine if repression of *cqsS* contributed to the remaining 6-fold drop in natural transformation, we deleted *luxO*. Deletion of *luxO* constitutively activates a high cell density expression profile regardless of CqsS activity or regulation. The 6-fold drop in natural transformation, caused by AphA in the presence of ectopic *tfoX* expression, was not altered by deleting *luxO* (compare grey and striped bars in Figure 5a).

Constitutive expression of AphA reduces levels of ComEA

Repression of VC0857 or *cqsS* cannot explain the lingering impact of AphA when *tfoX* is ectopically expressed. We resolved to determine which aspect of natural transformation was still impaired. As a starting point we measured DNA uptake. Hence, we incubated P_{tac}-*tfoX* cells with MFP488-labeled DNA and counted cells with DNA in their periplasm. Bacteria that constitutively expressed the non-functional N-terminally tagged AphA acquired DNA efficiently. Conversely, cells expressing functional C-terminally tagged AphA showed a significant 6-fold reduction (Figure 5d,e). Hence, DNA uptake was reduced by AphA even when TfoX was produced. Acquisition of DNA results from the

concerted activity of type IV pili and periplasmically localized ComEA, the latter of which acts as a molecular ratchet to facilitate DNA uptake [14,38,39). As we had already determined that pilus production was not affected by AphA in the P_{tac}-*tfoX* background (Figure 5c), we hypothesized that AphA may impact ComEA production. Using a functional fluorescent fusion, we found that ComEA expression was significantly reduced by expression of C-terminally tagged AphA (Figure 5d,e). Since AphA does not bind upstream of *comEA* (Figure S4) this repression must be indirect.

DISCUSSION

In *V. cholerae*, signals for natural competence are integrated at the *tfoX* promoter [4,5,14,31,40]. Triggers include: i) carbon starvation, mediated through CRP and ii) chitin-breakdown, sensed by membrane proteins ChiS and TfoS then communicated via the small RNA TfoR [5,6,7,31,41]. Regulatory links between cell density and competence are poorly characterised, although HapR has been shown to regulate genes required for internalisation of DNA, via the LuxR-family transcription factor QstR [11,42,43]. We propose that AphA directly couples competence to population density signals (Table 1, Figure 6). Mechanistically, AphA does this by preventing the activator CRP binding to the *tfoX* promoter (Figure 3). Hence, in low cell density populations, competence cannot be triggered. Our observations concerning AphA and CRP at the *tfoX* promoter are reminiscent of the *tcpPH* regulatory region. This locus also has overlapping sites for the two regulators that act antagonistically [44]. Opposing regulation was also observed at the *cqsS* promoter, although the regulators targeted distinct sites on the DNA (Figure 4). We speculate that antagonistic control of promoters by AphA and CRP is a common regulatory strategy in *V. cholerae*. At the *tfoX* promoter, the ability of AphA to displace CRP, even with the latter in excess, is of key importance. This ensures that *tfoX* expression cannot be switched on by carbon starvation and chitin metabolism alone; the bacterial population must also reach an appropriate density.

Unexpectedly, we found that AphA could interact with single DNA sites or co-operatively bind pairs of targets. In the examples tested here, binding a single site required the sequence to closely match the consensus for AphA binding (Figure 2). More divergent AphA sites could function in unison by co-operatively binding the regulator (Figure S2). These different configurations of DNA binding may explain why three previous studies each proposed a slightly different AphA binding consensus [24,26,27]. Unusually, none of these sequences were palindromic. We suggest that AphA preferentially binds to the inverted repeat sequence 5'-ATGCAA-N_4-TTGCAT-3' (Figure 1d). Consistent with this, structures of PadR family regulators demonstrate DNA binding as a dimer with two-fold symmetry [33]. Confusion likely arose previously because the sequence 5'-TGCA-3' is embedded as a direct repeat within the larger motif identified here (Figure 1d). Furthermore, a paucity of known AphA binding sites hindered prior studies.

Surprisingly, transcriptome analysis found only six differentially regulated operons in *V. cholerae* cells lacking *aphA*. Similar studies in *V. harveyi* identified hundreds of genes [22,25,45]. We speculate that these discrepancies result from the growth conditions used. This may also explain why control of the competence regulon was not identified. In particular, transcription of *tfoX* and *cqsS* requires CRP, but transcriptome analysis used rich media that triggers catabolite repression [45]. Indirectly, this would impact VC0857 that is induced by TfoX. Our data are consistent with transcriptome profiling of cells treated with quorum sensing molecules. Hence, VC0857, *tfoX* and *cqsS* are all activated by auto-inducers that block expression of AphA (Table 1). Similarly, like Rutherford and co-workers, we note that AphA frequently targeted genes involved in cell envelope physiology [22] . In hindsight, this is not surprising since the TCP is itself membrane associated [46]. Importantly, our ChIP-seq analysis did detect binding of AphA at the *tcpPH* locus, albeit at low levels (Figure S5). We were also able to detect AphA binding at its own promoter, consistent with previous reports of auto-regulation (Table 1) [22]. However, we did not detect AphA binding upstream of *pva* or *alsR*, the only other known targets [45,47].

In summary, our work better defines DNA binding by AphA and expands the direct regulon by >10-fold. Of particular interest are genes repressed by AphA that play key roles in the control of natural competence. Hence, as well as inducing the pathogenicity cascade at low population densities, AphA plays a key role by repressing genes utilised in the aquatic environment. We caution that our definition of the AphA regulon is unlikely to be complete. However, our work provides a solid basis for understanding changes in gene expression caused by transition of *V. cholerae* between the environmental niche and human host. In particular, we explain how competence can be controlled in this regard.

MATERIALS AND METHODS

Strains, plasmids and oligonucleotides

Standard procedures for cell culture and storage were used throughout. Strains were constructed using the approach of Dalia *et al.* [12]. Full descriptions of materials used are in Table S1. Derivatives of pRW50T were transferred from *E. coli* DH5α into *V. cholerae* by tripartite mating. Overnight cultures were washed twice using 0.9 % (*w/v*) NaCl, resuspended in LB, mixed in a 1:1:2 ratio of donor:recipient:helper, then spotted on non-selective LB plates. After overnight incubation at 30 ºC, cells were resuspended in 0.9 % NaCl and plated on TCBS agar containing 100 µg/ml streptomycin and 5 µg/ml tetracycline. After overnight incubation at 37 ºC, colonies were re-streaked on LB agar containing 100 µg/ml streptomycin and 5 µg/ml tetracycline. Conjugants were confirmed by PCR.

Chromatin immunoprecipitation

ChIP-seq experiments were done as described in Haycocks *et al.* [48]. Briefly, *V. cholerae* E7946 was transformed with plasmid pAMCF*aphA* or pAMNF*aphA*. These encode AphA with a C- or N-terminal

3xFLAG epitope respectively. The N-terminally tagged AphA was unable to bind DNA in ChIP-seq experiments and so served as a useful control. Note that levels of AphA produced from plasmid pAMCF*aphA* and the native chromosomal locus were indistinguishable (Figure S3). Cultures were incubated aerobically to mid-log phase in LB media at 37 ºC. Cells were cross-linked with 1 % (*v/v*) formaldehyde, washed, treated with lysozyme, and sonicated. The AphA-DNA complexes were immunoprecipitated with an anti-FLAG antibody (Sigma) and Protein A sepharose beads. Immunoprecipitated DNA was blunt-ended, A-tailed, and ligated to barcoded adaptors before elution and de-crosslinking. ChIP-seq libraries were then amplified by PCR and purified. Library quality was assessed using an Agilent Tapestation 4200 instrument and quantity determined by qPCR using an NEBnext library quantification kit (NEB).

Illumina sequencing and data analysis

Libraries were sequenced as previously described [49]. Each library was diluted to a concentration of 2 nM, before pooling and denaturation. Sequencing was done using an Illumina MiSeq instrument. Fastq files were deposited in Array Express (accession number E-MTAB-7953). Individual sequence reads were mapped against the *Vibrio cholerae* N16961 genome (Genbank accession numbers CP024162.1 and CP024163.1) using BWA (Burroughs-Wheeler Aligner) [50]. This facilitated comparison with other studies. Resulting Sequence Alignment Map (SAM) files were converted to Binary Alignment Map (BAM) files using the SAM-to-BAM tool [51,52]. Coverage per base was calculated using multiBAMsummary [53], and R was used to normalise each data set to the same overall read depth for each chromosome. To visualise the AphA binding profile coverage depth was plotted as a graph against genome features in Artemis. The graph window size was set to 100 bp and peaks with a coverage score of $\geq$ 10 over 300 consecutive bases were selected. The centre of the region passing the cut off was set as the peak centre. Next, 250 bp DNA sequences from each peak centre were collated. To identify DNA motifs associated with peak sequences we used MEME [54]. We scanned for motifs between 12 and 26 bp in length that occurred once per given sequence on the given DNA strand.

Natural transformation

Chitin-induced transformation assays of *V. cholerae* were done as described by using shrimp chitin flakes to induce competence (Sigma) [12]. Briefly, cells were grown to an OD_{600} of ~1 in LB. Cells in 1 ml of culture were recovered by centrifugation and washed twice with 1 ml 0.7 % (w/*v*) Instant Ocean (Aquarium Systems). Cells were diluted 10-fold with 0.7 % Instant Ocean and 1 ml added to 10 mg of sterile chitin in a 2 ml Eppendorf tube. After incubation at 30 ºC for 24 hours 200 ng of transforming DNA was added. Following a further 5 hours incubation cells were recovered in LB for 1-2 hours at 37 ºC with shaking. Cells were then plated for quantitative culture on selective media (to quantify the number of transformants) and non-selective media (to quantify the total viable counts). The transformation frequency is defined as the number of transformants divided by the total viable count in each reaction.

Protein purification and western blotting

V. cholerae CRP was purified using cAMP-agarose as previously described [55]. RNA polymerase was purified from *V. cholerae* N16961 using a protocol based on the method of Burgess and Jendrisak as previously described [55,56]. *V. cholerae* σ^{70} was purified by affinity chromatography as previously described [55]. To facilitate overexpression *aphA* was cloned in pET21a. The resulting plasmid was used to transform *E. coli* T7 Express cells. All colonies resulting from a single transformation were pooled and used to inoculate 500 ml of LB supplemented with 100 µg/ml ampicillin. Overexpression of C-terminally His_6 tagged AphA was induced with 1 mM IPTG for 3 hours. Cells were recovered by sonication and resuspended in 20 mM Tris-HCl pH 7.5, 1 mM EDTA pH 8.0, 10 mM NaCl and 1 mM PMSF. After cell lysis by sonication cell debris was removed by centrifugation and the lysate was passed through a His-Trap column (GE Healthcare). Proteins were eluted with a gradient of buffer containing 20 mM Tris-HCl pH 7.5, 1 mM EDTA pH 8.0, 10 mM NaCl and 500 mM imidazole. Fractions with AphA were identified by SDS-PAGE, pooled and concentrated. For long-term storage at -20 ^{o}C, glycerol was added to a final concentration of 50 % *(v/v)*. Western blots were done as described by Lamberte *et al.* [57].

Electrophoretic mobility shift assays (EMSAs)

DNA fragments for EMSA experiments were generated by PCR as previously described [58]. PCR products were cut using *Eco*RI and *Hin*dIII (NEB). End-labelling was done using γ^{32}-ATP and T4 polynucleotide kinase (NEB). Radiolabelled fragments were incubated with purified proteins in buffer containing 40 mM Tris acetate pH 7.9, 50 mM KCl, 5 mM $MgCl_2$, 500 µM DTT and 12.5 µg/ml Herring Sperm DNA for 15 minutes at 37 ^{o}C. Protein-DNA complexes were separated by electrophoresis using a 7.5 % non-denaturing polyacrylamide gel. Subsequently, dried gels were exposed to a Biorad phophorscreen that was scanned using a Biorad Personal Molecular Imager. Full gel images are shown in Figure S6.

DNAse I and $KMnO_4$ footprinting

DNA fragments were excised from pSR using *AatII-Hin*dIII. After end-labelling using γ^{32}-ATP and T4 PNK (NEB), footprints were done as previously described in buffer containing 40 mM Tris acetate pH 7.9, 50 mM KCl, 5 mM $MgCl_2$, 500 µM DTT and 12.5 µg/ml Herring Sperm DNA [59,60]. Resulting DNA fragments were analysed on a 6 % denaturing gel. Subsequently, dried gels were exposed to a Biorad phophorscreen that was scanned using a Biorad Personal Molecular Imager. Full gel images are shown in Figure S6.

In vitro *transcription assays*

We used the protocol of Kolb *et al.* [61] as described by Savery *et al.* [62]. Reactions contained different combinations of 16 µg/ ml supercoiled pSR template, *V. cholerae* RNA polymerase σ^{70} holoenzyme, AphA and CRP. In experiments where CRP was used, CRP was pre-incubated with cAMP 37 ^{o}C prior

to addition. The reaction buffer was 40 mM Tris pH 7.9, 5 mM $MgCl_2$, 500 µM DTT, 50 mM KCl, 100 µg/ ml BSA, 200 µM ATP/GTP/CTP, 10 µM UTP and 5 µCi α-P^{32}-UTP. If required, AphA and CRP were added to reactions for 10 minutes at 37 ºC before the addition of 0.4 µM RNA polymerase, for a further 10 minutes. Transcripts were analysed on a 6 % denaturing polyacrylamide gel. The dried gel was exposed to a Biorad Phosphorscreen, which was scanned using a Biorad Personal Molecular Imager. Full gel images are shown in Figure S6.

β-galactosidase assays

V. cholerae harbouring pRW50T were grown to mid-log phase (OD_{650} of ~1) in LB or M9 minimal media supplemented with 1 % fructose unless stated in figure legends. Cells were lysed using 1 % sodium deoxycholate and toluene, and assays carried out as previously described using the Miller method [55,63].

Microscopy

Strain P_{tac}-*tfoX* Δ*luxO* containing pAMCF*aphA* or pAMNF*aphA* was grown in continually rolling containers at 30 ºC to late-log phase in LB Miller broth supplemented with 50 µg/mL Kanamycin, 100 µM IPTG, 20 mM $MgCl_2$ and 10 mM $CaCl_2$. Around 10^8 colony-forming units (c.f.u.) were collected by centrifugation (18,000 x *g* for 1 minute) and resuspended in 0.7% Instant Ocean. Cells were then labelled with 25 µg/ml AlexaFluor488 maleimide (AF488-mal) in the dark for 15 minutes at room temperature. Cells were then washed twice with 0.7% Instant Ocean by sequential centrifugation and resuspension. Cells were imaged by time-lapse microscopy every 2 seconds for 2 minutes to monitor pilus production. The number of cells that made at least one pilus within the 2-minute window and the total number of cells were manually counted. To examine DNA internalisation, approximately 10^8 c.f.u. of late-log culture were diluted 4-fold with Instant Ocean. The cells were then incubated with or without 100 ng MFP488-labelled DNA at room temperature in the dark. After 30 minutes, 10 units of DNase I (NEB) was added to all reactions and incubated for 2 minutes to degrade any remaining extracellular DNA. Cells were then washed twice with 0.7% Instant Ocean by sequential centrifugation and resuspension. Static images of cells were taken and the number of cells with a DNA-uptake event, indicated by MFP-488 DNA foci, compared to the total number of cells in a field of view, was manually counted. For all microscopy experiments, samples were placed under 0.2 % Gelzan (Sigma) pads made with Instant Ocean medium. We used a Nikon Ti-2 microscope with a Plan Apo x60 objective, GFP and dsRed filter cubes and a Hamamatsu ORCAFlash4.0 camera. Image collection and analysis used Nikon NIS Elements imaging software and Image J.

ACKNOWLEDGEMENTS

This work was supported the Biotechnology and Biological Sciences Research Council (BBSRC) with grant BB/N005961/1 awarded to DCG and a PhD studentship awarded to LMW. The National Institutes

of Health supported ABD with grant R35GM128674. We would like to thank Joseph Wade for providing feedback on the manuscript prior to submission.

REFERENCES

1. Nelson EJ1, Harris JB, Morris JG Jr, Calderwood SB, Camilli A. 2009. Cholera transmission: the host, pathogen and bacteriophage dynamic. *Nat Rev Microbiol*. 2009 **7:**693-702.

2. Nalin DR, Daya V, Reid A, Levine MM, Cisneros L. 1979. Adsorption and growth of *Vibrio cholerae* on chitin. *Infect Immun*. **25:**768-70.

3. Jude BA, Martinez RM, Skorupski K, Taylor RK. 2009. Levels of the secreted *Vibrio cholerae* attachment factor GbpA are modulated by quorum-sensing-induced proteolysis. *J Bacteriol*. **191:**6911-6917.

4. Yamamoto S, Morita M, Izumiya H, Watanabe H. 2010. Chitin disaccharide (GlcNAc)2 induces natural competence in Vibrio cholerae through transcriptional and translational activation of a positive regulatory gene *tfoXVC*. *Gene*. **457:**42-9.

5. Yamamoto S, Izumiya H, Mitobe J, Morita M, Arakawa E, Ohnishi M, Watanabe H. 2011. Identification of a chitin-induced small RNA that regulates translation of the *tfoX* gene, encoding a positive regulator of natural competence in *Vibrio cholerae*. *J Bacteriol*. **193:**1953-1965.

6. Yamamoto S, Mitobe J, Ishikawa T, Wai SN, Ohnishi M, Watanabe H, Izumiya H. 2014. Regulation of natural competence by the orphan two-component system sensor kinase ChiS involves a non-canonical transmembrane regulator in *Vibrio cholerae*. *Mol Microbiol*. **91:**326-347.

7. Meibom KL, Blokesch M, Dolganov NA, Wu CY, Schoolnik GK. 2005. Chitin induces natural competence in *Vibrio cholerae*. *Science* **310:**1824-1827.

8. Metzger LC, Blokesch M. 2016. Regulation of competence-mediated horizontal gene transfer in the natural habitat of *Vibrio cholerae*. *Curr Opin Microbiol*. **30:**1-7.

9. Borgeaud S, Metzger LC, Scrignari T, Blokesch M. 2015. The type VI secretion system of *Vibrio cholerae* fosters horizontal gene transfer. *Science*. **347:**63-67.

10. Seitz P, Blokesch M. 2013. DNA-uptake machinery of naturally competent *Vibrio cholerae*. *Proc Natl Acad Sci* USA. **110:**17987-17992.

11. Lo Scrudato M, Blokesch M. 2012. The regulatory network of natural competence and transformation of *Vibrio cholerae*. *PLoS Genet*. **8:**e1002778.

12. Dalia AB, McDonough E, Camilli A. 2014. Multiplex genome editing by natural transformation. *Proc Natl Acad Sci* USA. **111:**8937-8942.

493 13. Ellison CK, Dalia TN, Vidal Ceballos A, Wang JC, Biais N, Brun YV, Dalia AB. 2018. Retraction
494 of DNA-bound type IV competence pili initiates DNA uptake during natural transformation in *Vibrio*
495 *cholerae*. *Nat. Microbiol*. **3:**773-780.

496 14. Seitz P, Pezeshgi Modarres H, Borgeaud S, Bulushev RD, Steinbock LJ, Radenovic A, Dal Peraro
497 M, Blokesch M. 2014. ComEA is essential for the transfer of external DNA into the periplasm in
498 naturally transformable *Vibrio cholerae* cells. *PLoS Genet*. **10:**e1004066.

499 15. Hay AJ, Zhu J. 2015. Host intestinal signal-promoted biofilm dispersal induces Vibrio cholerae
500 colonization. *Infect Immun*. **83:**317-323.

501 16. Childers BM, Klose KE. 2007. Regulation of virulence in *Vibrio cholerae*; the ToxR regulon. *Future*
502 *Microbiol* **2:**335-44.

503 17. Whiteley M, Diggle SP, Greenberg EP. 2017. Progress in and promise of bacterial quorum sensing
504 research. *Nature*. **551:**313-320.

505 18. Mukherjee S, Bassler BL. 2019. Bacterial quorum sensing in complex and dynamically changing
506 environments. *Nat Rev Microbiol*. doi:10.1038/s41579-019-0186-5. [Epub ahead of print].

507 19. Ng WL, Perez LJ, Wei Y, Kraml C, Semmelhack MF, Bassler BL. 2011. Signal production and
508 detection specificity in Vibrio CqsA/CqsS quorum-sensing systems. *Mol Microbiol*. **79:**1407-1417.

509 20. Eickhoff MJ, Bassler BL. 2018. SnapShot: Bacterial Quorum Sensing. *Cell*. **174:**1328-1328.

510 21. De Silva RS, Kovacikova G, Lin W, Taylor RK, Skorupski K, Kull FJ. 2005. Crystal structure of
511 the virulence gene activator AphA from *Vibrio cholerae* reveals it is a novel member of the winged
512 helix transcription factor superfamily. *J Biol Chem*. **280:**13779-13783.

513 22. Rutherford ST, van Kessel JC, Shao Y, Bassler BL. 2011. AphA and LuxR/HapR reciprocally
514 control quorum sensing in vibrios. *Genes Dev*. **25:**397-408.

515 23. Skorupski K, Taylor RK. 1999. A new level in the *Vibrio cholerae* ToxR virulence cascade: AphA
516 is required for transcriptional activation of the *tcpPH* operon. *Mol Microbiol*. **31:**763-771

517 24. Kovacikova G, Lin W, Skorupski K. 2004. *Vibrio cholerae* AphA uses a novel mechanism for
518 virulence gene activation that involves interaction with the LysR-type regulator AphB at the *tcpPH*
519 promoter. *Mol Microbiol*. **53:**129-142.

520 25. van Kessel JC, Rutherford ST, Shao Y, Utria AF, Bassler BL. 2013. Individual and combined roles
521 of the master regulators AphA and LuxR in control of the *Vibrio harveyi* quorum-sensing regulon. *J*
522 *Bacteriol*. **195:**436-443.

523 26. Sun F, Zhang Y, Wang L, Yan X, Tan Y, Guo Z, Qiu J, Yang R, Xia P, Zhou D. 2012. Molecular
524 characterization of direct target genes and cis-acting consensus recognized by quorum-sensing regulator
525 AphA in *Vibrio parahaemolyticus*. *PLoS One*. **7:**e44210.

27. Gu D, Liu H, Yang Z, Zhang Y, Wang Q. 2016. Chromatin Immunoprecipitation Sequencing Technology Reveals Global Regulatory Roles of Low-Cell-Density Quorum-Sensing Regulator AphA in the Pathogen *Vibrio alginolyticus*. *J Bacteriol*. **198:**2985-2999.

28. Ng D, Harn T, Altindal T, Kolappan S, Marles JM, Lala R, Spielman I, Gao Y, Hauke CA, Kovacikova G, Verjee Z, Taylor RK, Biais N, Craig L. 2016. The *Vibrio cholerae* Minor Pilin TcpB Initiates Assembly and Retraction of the Toxin-Coregulated Pilus. *PLoS Pathog*. **12:**e1006109.

29. Nguyen Y, Sugiman-Marangos S, Harvey H, Bell SD, Charlton CL, Junop MS, Burrows LL. 2015. Pseudomonas aeruginosa minor pilins prime type IVa pilus assembly and promote surface display of the PilY1 adhesin. *J Biol Chem*. **290:**601-611.

30. Papenfort K, Förstner KU, Cong JP, Sharma CM, Bassler BL. 2015. Differential RNA-seq of *Vibrio cholerae* identifies the VqmR small RNA as a regulator of biofilm formation. *Proc Natl Acad Sci* USA. **112:**E766-75.

31. Wu R, Zhao M, Li J, Gao H, Kan B, Liang W. 2015. Direct regulation of the natural competence regulator gene *tfoX* by cyclic AMP (cAMP) and cAMP receptor protein (CRP) in Vibrios. *Sci Rep*. **5:**14921.

32. Schultz SC, Shields GC, Steitz TA. 1991. Crystal structure of a CAP-DNA complex: the DNA is bent by 90 degrees. *Science*. **253:**1001-1007.

33. Park SC, Kwak YM, Song WS, Hong M, Yoon SI. 2017. Structural basis of effector and operator recognition by the phenolic acid-responsive transcriptional regulator PadR. *Nucleic Acids Res*. **45:**13080-13093.

34. Liang W1, Sultan SZ, Silva AJ, Benitez JA. 2008. Cyclic AMP post-transcriptionally regulates the biosynthesis of a major bacterial autoinducer to modulate the cell density required to activate quorum sensing. *FEBS Lett*. **582:**3744-3750.

35. Freeman JA, Bassler BL. 1999. A genetic analysis of the function of LuxO, a two-component response regulator involved in quorum sensing in *Vibrio harveyi*. *Mol Microbiol*. **31:**665-677.

36. Singh PK, Bartalomej S, Hartmann R, Jeckel H, Vidakovic L, Nadell CD, Drescher K. 2017. *Vibrio cholerae* Combines Individual and Collective Sensing to Trigger Biofilm Dispersal. *Curr Biol*. **27:**3359-3366.

37. Blokesch M, Schoolnik GK. 2008. The extracellular nuclease Dns and its role in natural transformation of *Vibrio cholerae*. *J Bacteriol*. **190:**7232-7240.

38. Gangel H, Hepp C, Müller S, Oldewurtel ER, Aas FE, Koomey M, Maier B. 2014. Concerted spatio-temporal dynamics of imported DNA and ComE DNA uptake protein during gonococcal transformation. *PLoS Pathog*. **10:**e1004043.

559 39. Hepp C, Maier B. 2016. Kinetics of DNA uptake during transformation provide evidence for a
560 translocation ratchet mechanism. *Proc Natl Acad Sci* USA. **113:**12467-12472.

561 40. Pollack-Berti A, Wollenberg MS, Ruby EG. 2010. Natural transformation of *Vibrio fischeri* requires
562 tfoX and tfoY. *Environ Microbiol*. **12:**2302-11.

563 41. Dalia AB, Lazinski DW, Camilli A. 2014. Identification of a membrane-bound transcriptional
564 regulator that links chitin and natural competence in *Vibrio cholerae*. *mBio*. **5:**e01028-13.

565 42. Jaskólska M, Stutzmann S, Stoudmann C, Blokesch M. 2018. QstR-dependent regulation of natural
566 competence and type VI secretion in *Vibrio cholerae*. *Nucleic Acids Res*. **46:**10619-10634.

567 43. Lo Scrudato M, Blokesch M. 2013. A transcriptional regulator linking quorum sensing and chitin
568 induction to render *Vibrio cholerae* naturally transformable. *Nucleic Acids Res*. **41:**3644-3658.

569 44. Kovacikova G, Skorupski K. 2001. Overlapping binding sites for the virulence gene regulators
570 AphA, AphB and cAMP-CRP at the *Vibrio cholerae tcpPH* promoter. *Mol Microbiol*. **41:**393-407.

571 45. Kovacikova G, Lin W, Skorupski K. 2005. Dual regulation of genes involved in acetoin biosynthesis
572 and motility/biofilm formation by the virulence activator AphA and the acetate-responsive LysR-type
573 regulator AlsR in *Vibrio cholerae*. *Mol Microbiol*. **57:**420-433.

574 46. Häse CC, Mekalanos JJ. 1998. TcpP protein is a positive regulator of virulence gene expression in
575 *Vibrio cholerae*. *Proc Natl Acad Sci USA*. **95:**730-734.

576 47. Kovacikova G, Lin W, Skorupski K. 2003. The virulence activator AphA links quorum sensing to
577 pathogenesis and physiology in *Vibrio cholerae* by repressing the expression of a penicillin amidase
578 gene on the small chromosome. *J Bacteriol*. **185:**4825-4836.

579 48. Haycocks JR, Sharma P, Stringer AM, Wade JT, Grainger DC. 2015. The molecular basis for control
580 of ETEC enterotoxin expression in response to environment and host. *PLoS Pathog*. **11:**e1004605.

581 49. Sharma P, Haycocks JRJ, Middlemiss AD, Kettles RA, Sellars LE, Ricci V, Piddock LJV, Grainger
582 DC. 2017. The multiple antibiotic resistance operon of enteric bacteria controls DNA repair and outer
583 membrane integrity. *Nat Commun*. **8:**1444.

584 50. Li H. Durbin, R. 2009. Fast and accurate short read alignment with Burrows-Wheeler Transform.
585 *Bioinformatics*. **25:**1754-1760.

586 51. Li H, Handsaker B, Wysoker A, Fennell T, Ruan J, Homer N, Marth G, Abecasis G, Durbin R; 1000
587 Genome Project Data Processing Subgroup. 2009. The Sequence Alignment/Map format and
588 SAMtools. *Bioinformatics*. **25:**2078-2079.

589 52. Afgan E, Baker D, Batut B, van den Beek M, Bouvier D, Čech M, Chilton J, Clements D, Coraor
590 N, Grüning B, Guerler A, Hillman-Jackson J, Jalili V, Rasche H, Soranzo N, Goecks J, Taylor J,

591 Nekrutenko A, Blankenberg D. 2018. The Galaxy platform for accessible, reproducible and
592 collaborative biomedical analyses: 2018 update. *Nucleic Acids Research* **46:**W537–W544.

593 53. Ramírez F, Ryan DP, Grüning B, Bhardwaj V, Kilpert F, Richter AS, Heyne S, Dündar F, Manke
594 T. 2016. deepTools2: a next generation web server for deep-sequencing data analysis. *Nucleic Acids*
595 *Res*. **44:**W160-5.

596 54. Bailey TL, Boden M, Buske FA, Frith M, Grant CE, Clementi L, Ren J, Li WW, Noble WS. 2009.
597 MEME SUITE: tools for motif discovery and searching. *Nucleic Acids Res*. **37:**W202-8.

598 55. Manneh-Roussel J, Haycocks JRJ, Magán A, Perez-Soto N, Voelz K, Camilli A, Krachler AM,
599 Grainger DC. 2018. cAMP Receptor Protein Controls *Vibrio cholerae* Gene Expression in Response to
600 Host Colonization. *mBio*. **9:**e00966-18.

601 56. Burgess RR, Jendrisak JJ. 1975. A procedure for the rapid, large-scale purification of *Escherichia*
602 *coli* DNA-dependent RNA polymerase involving Polymin P precipitation and DNA-cellulose
603 chromatography. *Biochemistry*. **14:**4634-4638.

604 57. Lamberte LE, Baniulyte G, Singh SS, Stringer AM, Bonocora RP, Stracy M, Kapanidis AN, Wade
605 JT, Grainger DC. 2017. Horizontally acquired AT-rich genes in *Escherichia coli* cause toxicity by
606 sequestering RNA polymerase. *Nat Microbiol*. **2:**16249.

607 58. Grainger DC, Goldberg MD, Lee DJ, Busby SJW. 2008. Selective repression by Fis and H-NS at
608 the *Escherichia coli dps* promoter. *Mol Microbiol*. **68:**1366–1377.

609 59. Chintakayala K, Singh SS, Rossiter AE, Shahapure R, Dame RT, Grainger DC. 2013. *E. coli* Fis
610 Protein Insulates the *cbpA* Gene from Uncontrolled Transcription. *PLoS Genet*. **9:**e1003152.

611 60. Singh SS, Grainger DC. 2013. H-NS Can Facilitate Specific DNA-binding by RNA Polymerase in
612 AT-rich Gene Regulatory Regions. *PLoS Genet*. **9:**e1003589.

613 61. Kolb A, Kotlarz D, Kusano S, Ishihama A. 1995. Selectivity of the *Escherichia coli* RNA
614 polymerase Eσ38 for overlapping promoters and ability to support CRP activation. *Nucleic Acids Res*.
615 **23:**819-826.

616 62. Savery NJ, Lloyd GS, Kainz M, Gaal T, Ross W, Ebright RH, *et al*. 1998. Transcription activation
617 at class II CRP-dependent promoters: identification of determinants in the C-terminal domain of the
618 RNA polymerase α subunit. *EMBO J*. **17:**3439-3447.

619 63. Miller JH. 1972. Experiments in molecular genetics. Cold Spring Harbor, NY, Cold Spring Harbor
620 Laboratory Press.

621 64. Herzog R, Peschek N, Fröhlich KS, Schumacher K, Papenfort K. 2019. Three autoinducer
622 molecules act in concert to control virulence gene expression in *Vibrio cholerae*. *Nucleic Acids Res*.
623 **47:**3171-3183.

624 65. Levine MM, Black RE, Clements ML, Cisneros L, Saah A, Nalin DR, Gill DM, Craig JP, Young
625 CR, Ristaino P. 1982. The pathogenicity of nonenterotoxigenic *Vibrio cholerae* serogroup O1 biotype
626 El Tor isolated from sewage water in Brazil. *J Infect Dis*. **145:**296-299

627 66. Taylor RG, Walker DC, McInnes RR. 1993. *E. coli* host strains significantly affect the quality of
628 small scale plasmid DNA preparations used for sequencing. *Nucleic Acids Res*. **21:**1677-1678.

629 67. Connell TD, Martone AJ, Holmes RK. 1995. A new mobilizable cosmid vector for use in *Vibrio*
630 *cholerae* and other gram-negative bacteria. *Gene*. **153:**85-87.

631 68. Page L, Griffiths L, Cole JA. 1990. Different physiological roles of two independent pathways for
632 nitrite reduction to ammonia by enteric bacteria. *Arch Microbiol*. **154:**349-354.

633 69. Hayes, C. A., Dalia, T. N. and Dalia, A. B. 2017. Systematic genetic dissection of chitin
634 degradation and uptake in *Vibrio cholerae*. *Environ Microbiol*. **19**: 4154-4163.

Table 1: Position and sequence of AphA binding sites across the *V. cholerae* genome

Peak Centre[1]	Motif centre[2]	Motif sequence (5' to 3')[3]	Gene(s)[4]	Adjacent gene(s)[5]
		Chromosome I		
99851	99843	ctatgaaattaaattaataa	VC0102[a]	VC0102[a]
331346	331333	gtagtcgagcagttgcttac	(VC0317)	
371706	371662	ggatgcaacaggtcgattgg	(VC0348)	VC0349
423066	423063	ctatgcaacaatctgcgcct	(VC0397)	VC0398
519136	519147	caatgcaactgctctcttac	(VC0487)	
707906	707923	ctaagcagcgaaatgcatac	VC0661 < > VC0662[r]	VC0661 < > VC0662[r]
924229	924216	ctatgcaagttgattcatca	VC0857[a] < > VC0858	VC0857[a] < > VC0858
929346	929341	gcaggcgccctgttgcatag	(VC0864)	
936166	936182	ctattcaacaagtttccaca	(VC0870)	
1046511	1046514	cgcagcatccaattgcattg	(VC0982)	VC0982
1090236	1090207	ctatgcaacataatcaatct	VC1020 < > VC1021	VC1020 < > VC1021
1154126	1154085	ctatgcaggtgattgcagaa	(VC1086)[a]	VC1087
1224784	1224685	ccatgcattttaccgattac	VC1152 < > VC1153[a]	VC1152 < > VC1153[a]
1638101	1637985	caagtcgtagtgatgctcac	(VC1522)	VC1522 < > VC1523[a]
1656711	1656747	ctgagcatactgttgcatcc	(VC1543)	
1882301	1882329	ttgctcactgagtttcatac	(VC1746), (VC1747)	VC1746 < > VC1747
2234986	2234972	ggttgcaacggtttgaatac	(VC2077)	
2327841	2327831	atatgaagctatttgctggt	(VC2183)	VC2183
2364316	2364236	ccatgcgcttgattgcaagt	VC2211 < > VC2212[r]	VC2211 < > VC2212[r]
2435536	2435532	ctaagaagccgagtgcataa	VC2280	VC2280
2466111	2466116	agatgcaaattgttgcatct	VC2317	VC2317
2568506	2568491	gttttaaatctgttgcatac	(VC2400)	VC2339
2628331	2628303	ctgtgaacctagacgcatgg	(VC2448)	VC2447
2690451	2690442	accggcaacatgatgcagcc	(VC2503)	
2762401	2762392	acgagcaacaagttgcgcgt	(VC2593)	VC2592
2810891	2810831	gcatgaaacgtattgctggc	(VC2638)	
2821251	2821257	gtattccactttatgcttat	VC2647[r]	VC2647[r]
2926246	2926235	tctctcaactcaatgcatac	(VC2750)	VC2751
		Chromosome II		
39905	39881	cttatctacttgatgcatag	VCA0032[a]< >VCA0033	VCA0032[a]< >VCA0033
71933	71948	ggctgcatcagtttgcttac	(VCA0064)[r]	
83056	83013	gtaggaatttcatttcatac	(VCA0074)[r]	
105925	105897	gtatgaaaccttagtcatgg	(VCA0098)	
180601	180618	ctctgcatccagatgcagga	(VCA0162)	VCA0163
215501	215472	tcattcaagcgtttgcatag	(VCA0198)[r]	VCA0199
220027	219980	tgtggaaacttgttgaatag	(VCA0202)	
270051	270033	catttccacaggtttcataa	VCA0294[a]	VCA0294[a]
292440	292420	tgtggaaacttgttgaatag	(VCA0275)	
310741	310644	ctatggtttttttgcatag	VCA0291	VCA0291
354757	354789	ctatgcgctttttgcttag	VCA0367[a]	VCA0367[a]
428574	428600	ctattcaacaagtttccaca	(VCA0493)	VCA0494
454719	454697	atgtgcatgttgatgattag	VCA0522[a]	VCA0522[a]
772158	772161	caatgcaaccaaatgaacag	VCA0826	VCA0826
802525	802499	cgcatcaatcagttgcatct	(VCA0851)	
897851	897797	gcgtgcacaataattcatat	VCA0946[a]	VCA0946[a]
908441	908327	acgtgccaacttttcattag	VCA0959	VCA0959
1035131	1035098	gaattaaatcaatttcatat	(VCA1081)	
1052121	1052131	ctatccaacatgttgcgtat	(VCA1095)[a]	
1053076	1053158	atagtcaaccattttcctac	(VCA1097)	VCA1097 < > VCA1098
1056176	1056200	ctactcaacatgttgctggc	(VCA1100)	

[1]The centre of the ChIP-seq peak was defined as the centre of the 300 bp region that passed out cut-off for peak selection. Co-ordinates are for the *Vibrio cholerae* N16961 genome.
[2]Centre of AphA binding site associated with each peak. Note that these are predictions generated by MEME.
[3]Sequence of the predicted AphA binding site generated by MEME.
[4]Indicates the position of the peak with respect to the nearest gene(s). If the gene name is bracketed then the peak falls within the gene. Otherwise the peak is upstream of the gene or between divergent (< >) genes. Those genes activated[(a)] or repressed[(r)] by the presence of quorum sensing molecules AI-2, DPO and CAI-1 are indicated [64]. Note that the auto-inducer molecules drive down levels of AphA and so have the opposite regulatory effect.
[5]This column indicates the gene(s) with the closest start codon to the peak. In many cases peaks within genes are close to a start codon of an adjacent gene. If no gene name is given then the peak centre is not close to a start codon. Those genes activated[(a)] or repressed[(r)] by the presence of quorum sensing molecules AI-2, DPO and CAI-1 are indicated [64]. Note that the auto-inducer molecules drive down levels of AphA and so have the opposite regulatory effect.

FIGURE LEGENDS

Figure 1: Genome-wide binding of AphA in *Vibrio cholerae*

a. Binding of AphA across both *Vibrio cholerae* chromosomes. In each plot the outer two tracks (blue) are genes orientated in the forward or reverse direction. The AphA ChIP-seq binding signal (teal) is the inner profile. Position 1 of each chromosome is denoted by the tick mark at the top of each plot. Further tick marks are 1 Mbp apart.

b. Position of AphA binding peaks with respect to genes. The histogram shows the distribution of AphA binding peak centres with respect to the start codon of the nearest gene. The pie chart shows the proportion of binding peaks in coding or non-coding DNA.

c. Example AphA ChIP-seq binding peaks. The panel illustrates intragenic AphA binding peaks close to a gene (block arrow) start codons. ChIP-seq coverage plots are shown for individual experimental replicates. Data for AphA are in teal and control profiles are grey. Signals above or below the horizontal line correspond to reads mapping to the top or bottom strand respectively.

d. Sequence motif derived from AphA binding peaks using MEME.

e. Distances between AphA binding peak centres and motifs. Data are shown as a histogram. The AphA motif is that shown in panel d. The control motif was identified by MEME as lacking statistical significance.

f. Pie chart showing gene classes targeted by AphA.

Figure 2: Repression of VC0857 expression by AphA.

a. AphA binding between VC0857 and V0858. Genes are shown as block arrows. ChIP-seq coverage plots are shown for individual experimental replicates. Data for AphA are in teal and control profiles are grey. Signals above or below the horizontal line correspond to reads mapping to the top or bottom strand respectively.

b. DNA sequence of the intergenic region between VC0857 and VC0858. For clarity, the sequence orientation has been inverted. Coding DNA sequence is light green. Bent arrows denote transcription start sites for VC0857 (solid line) and VC0858 (broken line). Promoter elements are labelled similarly. Distances (bp) are with respect to the VC0857 transcription start site. The teal asterisk denotes the ChIP-seq peak centre. The AphA binding site is boxed and labelled.

c. DNase I footprint of AphA bound at the intergenic region. Lane 1 is a Maxim-Gilbert 'G+A' ladder. Lane 2 shows the pattern of DNase I cleavage in the absence of AphA. Lanes 3-6 show the DNase I cleavage at increasing concentrations of AphA (0.25, 0.50, 1.00 and 2.00 μM). The AphA footprint is indicated with a vertical teal bar.

d. AphA prevents RNA polymerase binding. Electrophoretic mobility shift assay showing mobility the VC0857-VC0857 intergenic DNA (lane 1), with 0.5 μM AphA (lane 2), 0.4 μM RNA polymerase (lane 3), or both factors (lane 4).

e. AphA represses VC0857 *in vitro*. The gel shows the result of an *in vitro* transcription experiment. The DNA template was plasmid pSR containing the VC0857 promoter and regulatory region. Experiments were done with 0.4 μM RNA polymerase in the absence (lane 1) or presence (lane 2) of 1 μM AphA . The RNAI transcript is plasmid-derived and acts as an internal control. The VC0857 transcript is labelled.

f. Activity of the VC0857 promoter *in vivo*. β-galactosidase activity was measured in cell lysates taken from *Vibrio cholerae* E7946 (solid teal line) or the Δ*aphA* derivative (broken teal line) containing the VC0857 promoter cloned upstream of *lacZ* in pRW50T. Ectopic expression of *tfoX* was provided by plasmid pMMB-*tfoX*. This is necessary because no VC0857 promoter activity is detectable in the absence of *tfoX*. Standard deviation is shown for three independent biological replicates. Cells were grown in LB supplemented with 1 mM IPTG.

g. Model for AphA-mediated repression at VC0857. AphA binds a single site overlapping the VC0857 promoter and occludes RNA polymerase binding.

Figure 3: Repression of *tfoX* expression by AphA.

- **a.** AphA binds at the *tfoX* locus *in vivo*. Genes are shown as block arrows. ChIP-seq coverage plots are shown for individual experimental replicates. Data for AphA are in teal and control profiles are grey. Signals above or below the horizontal line correspond to reads mapping to the top or bottom strand respectively.
- **b.** DNA sequence of the *tfoX* regulatory region. The -35 and -10 elements are underlined and labelled, and the transcription start site is shown as a bent arrow. Distances are with respect to the *tfoX* transcription start site. The CRP binding site is orange and AphA sites are boxed. The ChIP-seq peak centre is denoted by an asterisk. Red bases above the sequence indicate mutations made to each AphA site.
- **c.** Binding of AphA and CRP to overlapping sites at the *tfoX* promoter. The gel shows the result of DNase I footprinting experiment. The gel is calibrated with a Maxim/Gilbert 'G+A' ladder in lane 1. The pattern of DNase I cleavage in the absence of any proteins is in lane 2. Protection of DNA from DNase I cleavage in the presence of 0.5 µM CRP is shown in lane 3 and highlighted by the vertical yellow bar. Sites of DNAse I hypersensitivity due to CRP binding are indicated by yellow triangles. Protection from DNase I cleavage in the presence of 1.0 µM AphA is shown in lane 4 and is highlighted by vertical teal bars. Increased DNase I cleavage induced by AphA is indicated by a teal triangle. In the presence of 0.5 µM CRP, increasing concentrations of AphA result in the replacement of the CRP footprint with an AphA footprint (lanes 5-9, AphA concentrations: 0, 0.5 µM, 1.0 µM, 2.0 µM, 3.0 µM).
- **d.** AphA outcompetes CRP for binding at the *tfoX* locus. Electrophoretic mobility shift assay showing the mobility of the *tfoX* promoter fragment alone (lane 1), in the presence of 0.5 µM AphA (lane 2), 1.0 µM CRP (lane 3), or both proteins (lane 4).
- **e.** AphA antagonises CRP-dependent transcription activation at the *tfoX* promoter *in vitro*. The gel shows transcripts derived from a pSR based DNA template containing the *tfoX* promoter region. The *tfoX* and RNAI (control) transcripts are labelled. Lane 1 shows transcripts produced in the absence of CRP or AphA. Transcription from the *tfoX* promoter increased in the presence of CRP (lanes 3-7: 1, 3, 5 µM CRP). Addition of AphA with 3 µM CRP reduced *tfoX* transcription (lanes 5-8, concentrations of AphA: 0, 1, 3, 5 µM).
- **f.** AphA regulates *tfoX* transcription *in vivo*. β-galactosidase activity was measured in lysates of *Vibrio cholerae* E7946 (solid teal line) or the Δ*aphA* derivative (broken teal line) containing the *tfoX* promoter cloned upstream of *lacZ* in pRW50T. Standard deviation is shown for three independent biological replicates. Cells were grown in LB medium.
- **g.** Model for AphA repression of *tfoX*. CRP activates transcription from the *tfoX* promoter in the absence of AphA. At low cell density, AphA co-operatively binds two adjacent sites to displace CRP.

Figure 4: Interactions between AphA, CRP and the *cqsS* regulatory region.

- **a.** AphA binds upstream of *cqsS in vivo*. Genes are shown as block arrows. ChIP-seq coverage plots are shown for individual experimental replicates. Data for AphA are in teal and control profiles are grey. Signals above or below the horizontal line correspond to reads mapping to the top or bottom strand respectively.
- **b.** Sequence of the *cqsS* intergenic region. Coding DNA is in blue. Promoter elements are underlined and labelled. The transcription start site is shown as a bent arrow. Distances are with respect to the *cqsS* transcription start site. The CRP binding site is in orange and AphA binding sites are boxed. The centre of the AphA ChIP-seq peak is denoted by a teal asterisk. Mutations introduced into each AphA site are shown in red above the sequence.
- **c.** AphA and CRP bind distinct sites at P*cqsS*. The gel shows the result of a DNase I footprint using a DNA fragment containing P*cqsS*. A Maxim-Gilbert 'G+A' ladder has been used to calibrate the gel (lane 1). Lane 2 shows the pattern of DNase I cleavage in the absence of AphA. The addition of 3 µM CRP produces a footprint indicated by the yellow vertical bar (lane 3).

The vertical teal bar indicates the footprint formed in the presence of 1 µM AphA (lane 4). The CRP footprint is not altered by increasing concentrations of AphA (lanes 5-7, CRP concentration: 3 µM, AphA concentrations: 1, 2, 3 µM).

d. AphA and CRP bind to P*cqsS* simultaneously. The gel shows the result of electrophoretic mobility shift assay using a DNA fragment containing P*cqsS*. Data are shown for the DNA alone (lane 1), or in the presence of 1 µM AphA (lane 2), 3 µM CRP (lane 3), or both proteins (lane 4).

e. AphA and CRP have antagonistic effects on P*cqsS in vitro*. Result of an *in vitro* transcription experiment using the P*cqsS* promoter cloned in pSR as a template. Reactions all contained 0.4 µM RNA polymerase. Transcription factors were added as follows: 3 µM CRP (lane 2), 1 µM AphA (lane 3) 3 µM CRP, and 1, 2, or 3 µM AphA (lanes 4-6).

f. Opening of the *cqsS* promoter by RNA polymerase is controlled by CRP and AphA. The gel shows the result of a $KMnO_4$ footprint. A Maxim/Gilbert 'G+A' reaction is shown in lane 1 for calibration. Lane 2 shows an absence of DNA opening without added proteins. Addition of 3 µM CRP (lane 3), 1 µM AphA (lane 4), or 300 nM RNA polymerase (lane 5) alone does not impact DNA melting. In the presence of 3 µM CRP and 300 nM RNA polymerase promoter unwinding was observed (lane 6). This was inhibited by AphA (lanes 7-9, AphA concentrations: 1, 2 and 3 µM).

g. Activity of P*cqsS in vivo*. β-galactosidase activity was measured using cell lysates taken from *Vibrio cholerae* E7946 (solid teal line) or the Δ*aphA* derivative (broken teal line) containing P*cqsS* cloned upstream of *lacZ* in pRW50T. Standard deviation is shown for three independent biological replicates. Cells were grown in M9 minimal media supplemented with 0.3 % (*w/v*) fructose.

h. Model for AphA-mediated repression at P*cqsS in vitro*. CRP activates transcription from a site centred at position -41.5 relative to the *cqsS* transcription start site. AphA binds to two sites overlapping the transcription start site to repress transcription.

Figure 5: AphA represses DNA uptake *in vivo* by repressing expression of TfoX and ComEA.

a. Chitin-induced transformation assays at low and high cell density. The $LuxO^{D47E}$ derivative is constitutively active due to a phosphomimetic mutation that locks *V. cholerae* in a low cell density state. The *dns* gene encodes an endonuclease expressed at low (but not high) cell density to degrade DNA obtained by natural transformation. P_{tac}-*tfoX* is a chromosomally integrated IPTG-inducible construct. Transformation reactions for strains with P_{tac}-*tfoX* were supplemented with 100 µM IPTG. Plasmid encoded N- (N-FLAG) or C-terminally (C-FLAG) tagged AphA was constitutively expressed in strains as indicated. Transforming DNA was an antibiotic resistance cassette that integrates in place of VC1807 encoding Erm^R, Zeo^R or Tet^R. All data are from at least 4 independent biological replicates and P was calculated using a two-tailed Student's t-test. Data were significant at * $P \leq 0.05$; ** $P \leq 0.01$ or *** $P \leq 0.001$.

b. Pilus production was assessed by timelapse microscopy using cells labelled with AF488-mal. Data are representative of at least 3 independent experiments. White arrows indicate dynamic pilus events and arrow orientation indicates extension or retraction. The scale bar is 1 µm.

c. Quantification of pilus dynamic activity (as shown in b) as the percentage of cells that exhibited at least 1 dynamic pilus event. Data are from three independent experiments and n = 527 cells analysed for N-FLAG and n = 625 for C-FLAG.

d. Uptake of MFP488-labelled DNA was assessed in *comEA*-mCherrry, Ptac-*tfoX*, Δ*luxO* cells harbouring plasmids for constitutive expression of N- or C- terminally tagged AphA as indicated. Data are representative of at least 3 independent experiments. The scale bar is 1µm.

e. Quantification of DNA uptake (as shown in d) by assessing the percentage of cells that displayed periplasmically localized MFP488-labelled DNA. Data are from three independent experiments and n = 1227 cells analysed for N-FLAG and n = 1138 for C-FLAG. P = 0.002 (two tailed Student's t-test).

f. Quantification of ComEA-mCherry expression by measuring mCherry fluorescence in a microplate reader. Data are from four independent biological replicates. P = 0.0002 (two-tailed Student's t-test).

Figure 6: Model for AphA-dependent regulation of natural competence. The diagram illustrates regulatory pathways controlling the induction of natural competence. Solid and dashed arrows represent direct and indirect activation respectively. Barred lines indicate repression. Proteins are shown as ovals and spheres whilst genes are shown as arrows. Nucleic acids are shown as grey (DNA) or peach (RNA) wavy lines. The DNA uptake machinery comprises PilABCD, PilQPONM, ComEA, ComEC, VC0857 and VC0858 (encoding the minor pilins). Repression of competence by AphA primarily occurs at the level of *tfoX* repression. A small number of factors and intermediary steps have been omitted for clarity.

SUPPLEMENTARY FIGURE LEGENDS

Figure S1: Binding of AphA to different DNA fragments *in vitro*. The gel images show results of electrophoretic mobility shift assay using DNA fragments corresponding to the indicated intergenic DNA regions. The *lacZ* promoter region used was from *E. coli* whilst other DNA fragments were derived from *V. cholerae*.

Figure S2: Binding of AphA to the *tfoX* and *cqsS* regulatory regions.

a. Binding of AphA to the *tfoX* regulatory region and derivatives. The gel shows the result of a DNase I footprint using a DNA fragments containing the *tfoX* regulatory region or derivatives with point mutations in individual AphA sites. Lanes 1-4 show results for the wild type DNA fragment. Lanes 5-7 and 8-10 show results with AphA I or AphA II mutated respectively. A Maxim-Gilbert 'G+A' ladder has been used to calibrate the gel (lane 1). Lanes 2, 5 and 8 show the pattern of DNase I cleavage in the absence of AphA. Where added, AphA was present at concentrations of 0.5 or 1.0 μM.
b. Binding of AphA to the *cqsS* regulatory region and derivatives. The gel shows the result of a DNase I footprint using a DNA fragments containing the *cqsS* regulatory region or derivatives with point mutations in individual AphA sites. Lanes 1-4 show results for the wild type DNA fragment. Lanes 5-7 and 8-10 show results with AphA I or AphA II mutated respectively. A Maxim-Gilbert 'G+A' ladder has been used to calibrate the gel (lane 1). Lanes 2, 5 and 8 show the pattern of DNase I cleavage in the absence of AphA. Where added, AphA was present at concentrations of 2.0 or 3.0 μM.

Figure S3: Levels of chromosomal and plasmid encoded AphA are indistinguishable.

a. Image of a western blot to compare levels of AphA3xFLAG generated from the native chromosomal locus for *aphA* (lanes 2-4) and from plasmid pAMCF*aphA* (lanes 5-7). Individual lanes are replicates and equal amounts of total cellular protein were loaded in each lane. Cultures were harvested at an OD_{650} of 0.6.
b. Quantification of relative AphA3xFLAG levels. The AphA3xFLAG band intensity for each lane in panel a was determined using Quantity One software. The average band intensity is shown and error bars represent the standard deviation of the three experimental replicates shown in panel a. P=0.299 was calculated using a two-tailed Student's t-test and there was no significant difference in AphA levels when comparing the two expression methods (NS).

Figure S4: AphA does not bind to the *comEA* regulatory region *in vivo*. Genes are shown as block arrows. ChIP-seq coverage plots are shown for individual experimental replicates. Data for AphA are in teal and control profiles are grey. Signals above or below the horizontal line correspond to reads mapping to the top or bottom strand respectively.

Figure S5: AphA binds to the *tcpPH* regulatory region *in vivo*.

a. ChIP-seq data for AphA binding at the *tcpPH* locus. Genes are shown as block arrows. ChIP-seq coverage plots are shown for individual experimental replicates. Data for AphA are in teal and control profiles are grey. Signals above or below the horizontal line correspond to reads mapping to the top or bottom strand respectively.
b. Sequence of the *tcpPH* intergenic region. Coding DNA is in blue. Promoter elements are underlined and labelled. The transcription start site is shown as a bent arrow. Distances are with respect to the *tcpPH* transcription start site. The centre of the AphA ChIP-seq peak is denoted by a teal asterisk. The known AphA binding site is boxed.

Figure S6: Raw gel images. Complete raw gel images are shown and subsections of images used for figures are indicated.

Movie S1: Pilus dynamics in the presence of AphA with an N-terminal 3xFLAG fusion. To monitor pilus dynamics, we utilised *V. cholerae* encoding PilA^{S67C}. The cysteine substitution facilitates *in vivo* labelling of PilA with the fluorescent dye AF488-mal. The strain used is P_{tac}-*tfoX*, Δ*luxO*, *comEA*-mCherry and harbours the pAMNF*aphA* vector.

Movie S2: Pilus dynamics in the presence of AphA with a C-terminal 3xFLAG fusion. To monitor pilus dynamics, we utilised *V. cholerae* encoding PilA^{S67C}. The cysteine substitution facilitates *in vivo* labelling of PilA with the fluorescent dye AF488-mal. The strain used is P_{tac}-*tfoX*, Δ*luxO*, *comEA*-mCherry and harbours the pAMCF*aphA* vector.

Figure 1

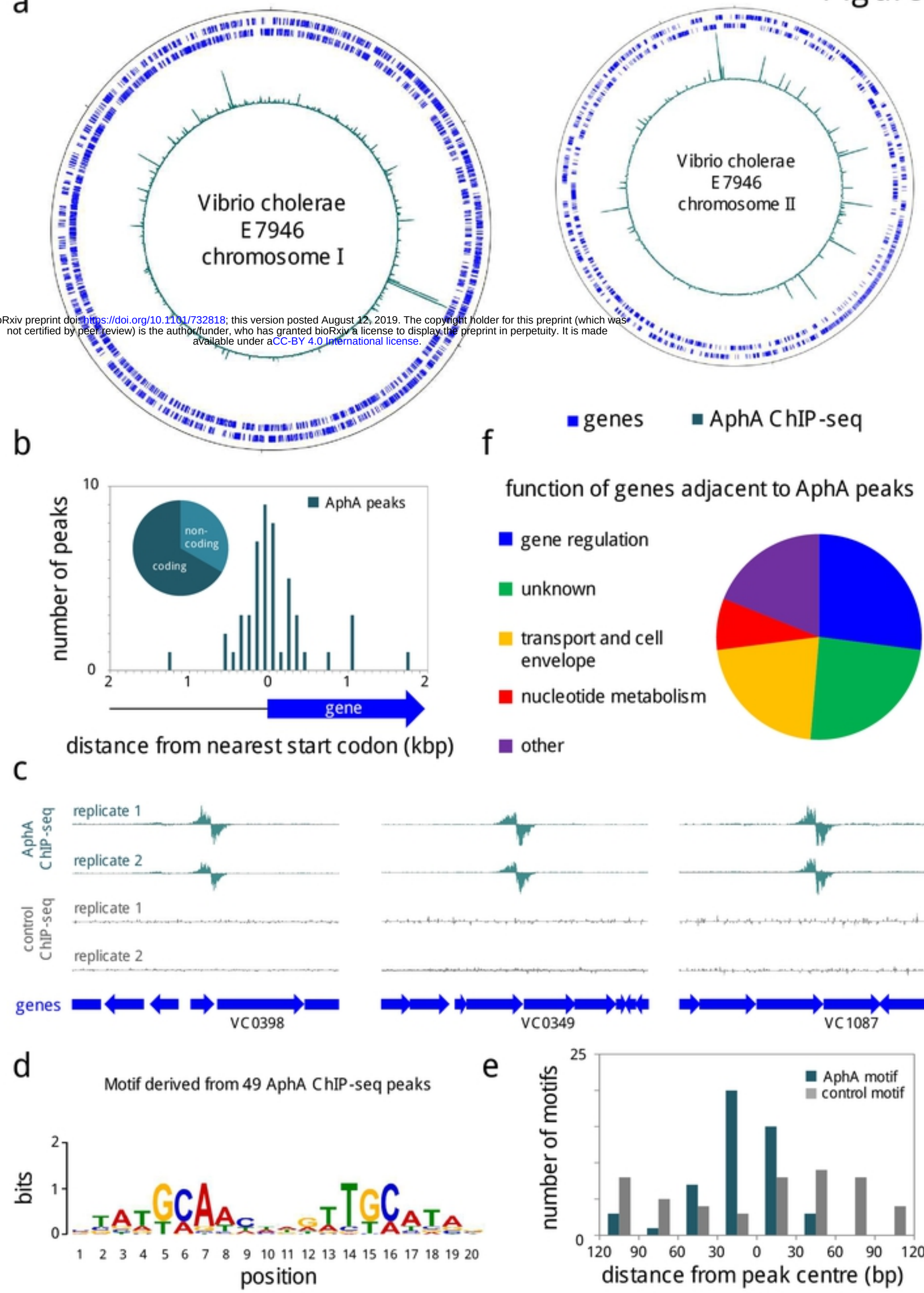

Figure 2

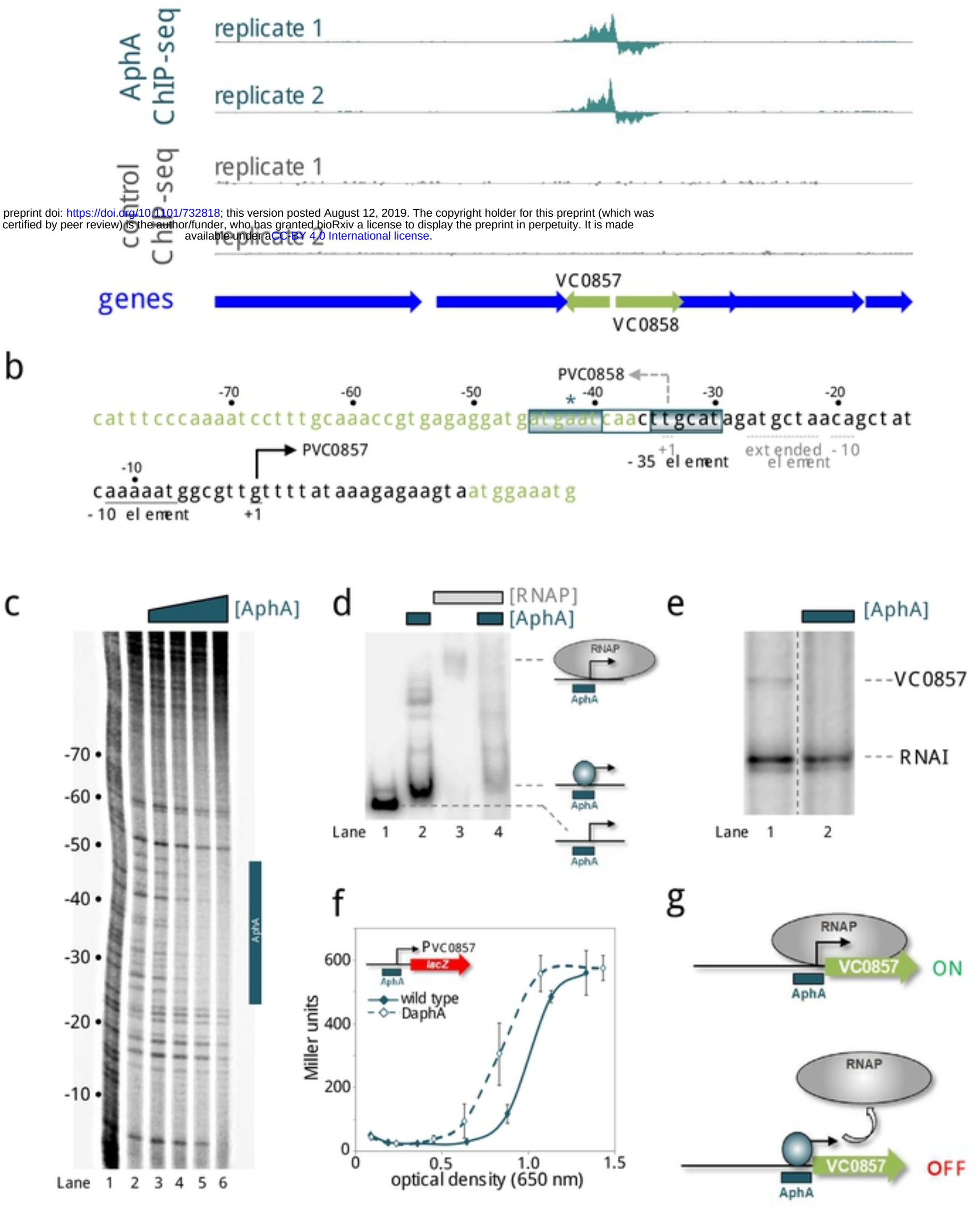

Figure 3

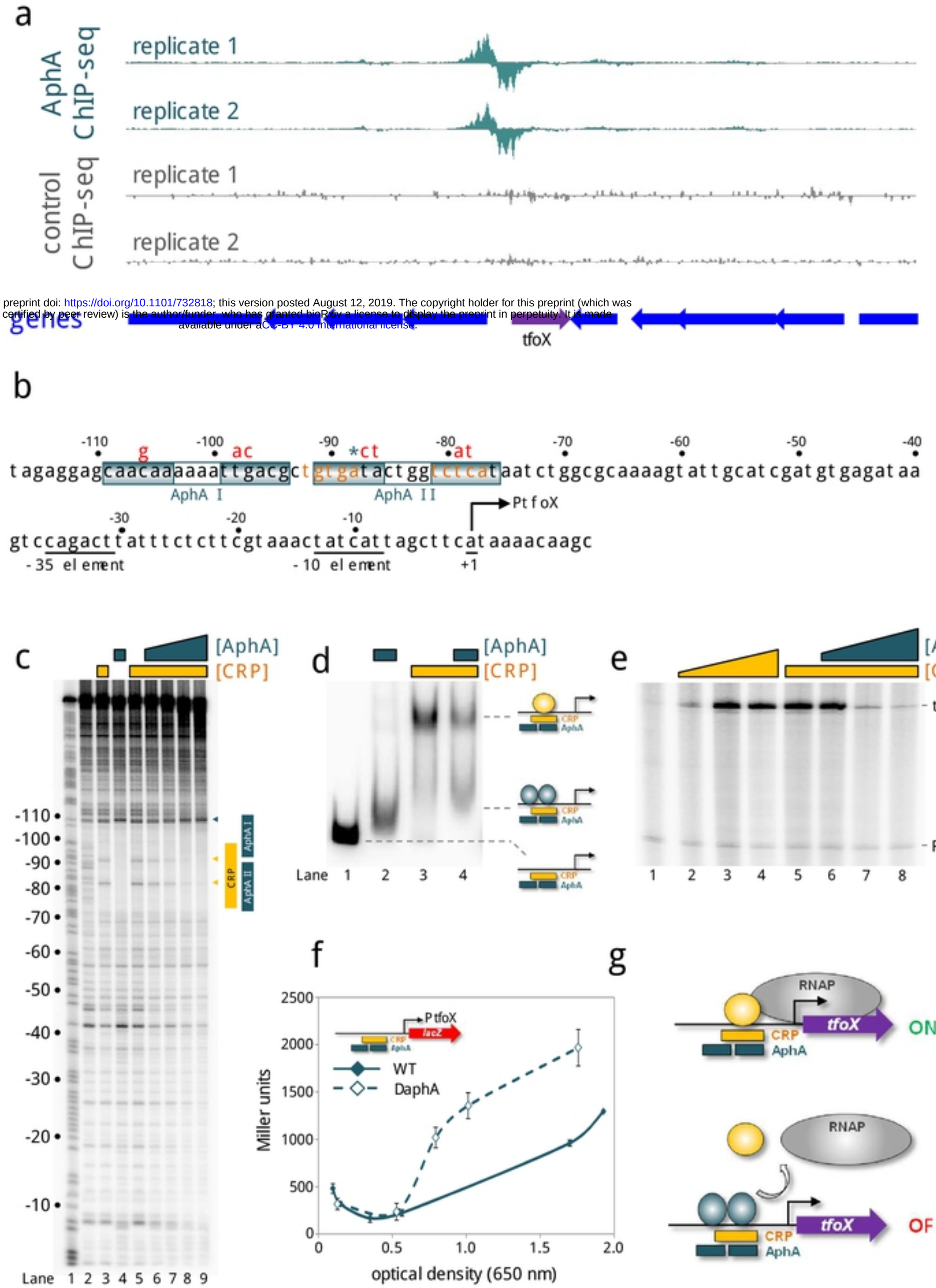

Figure 4

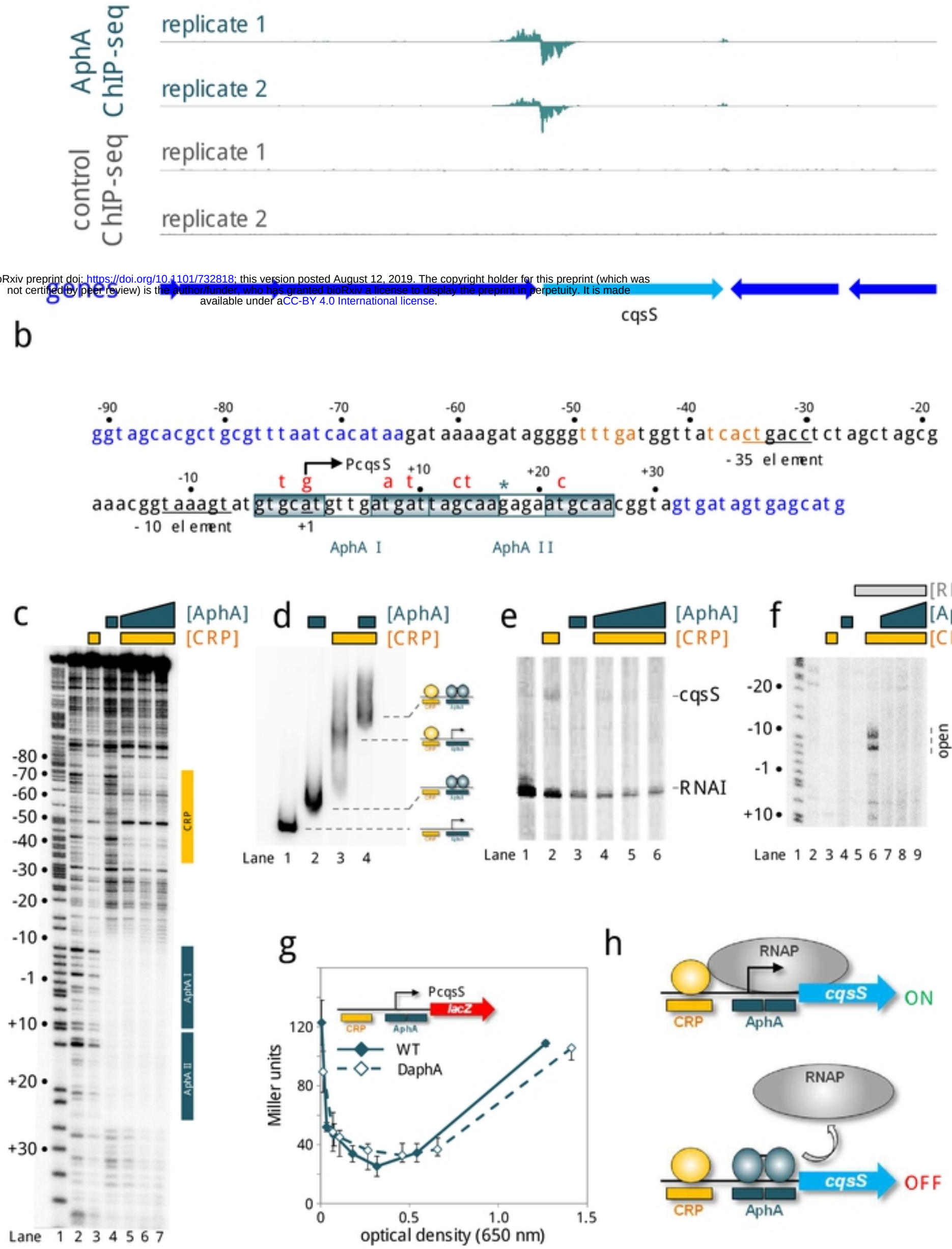

Figure 5

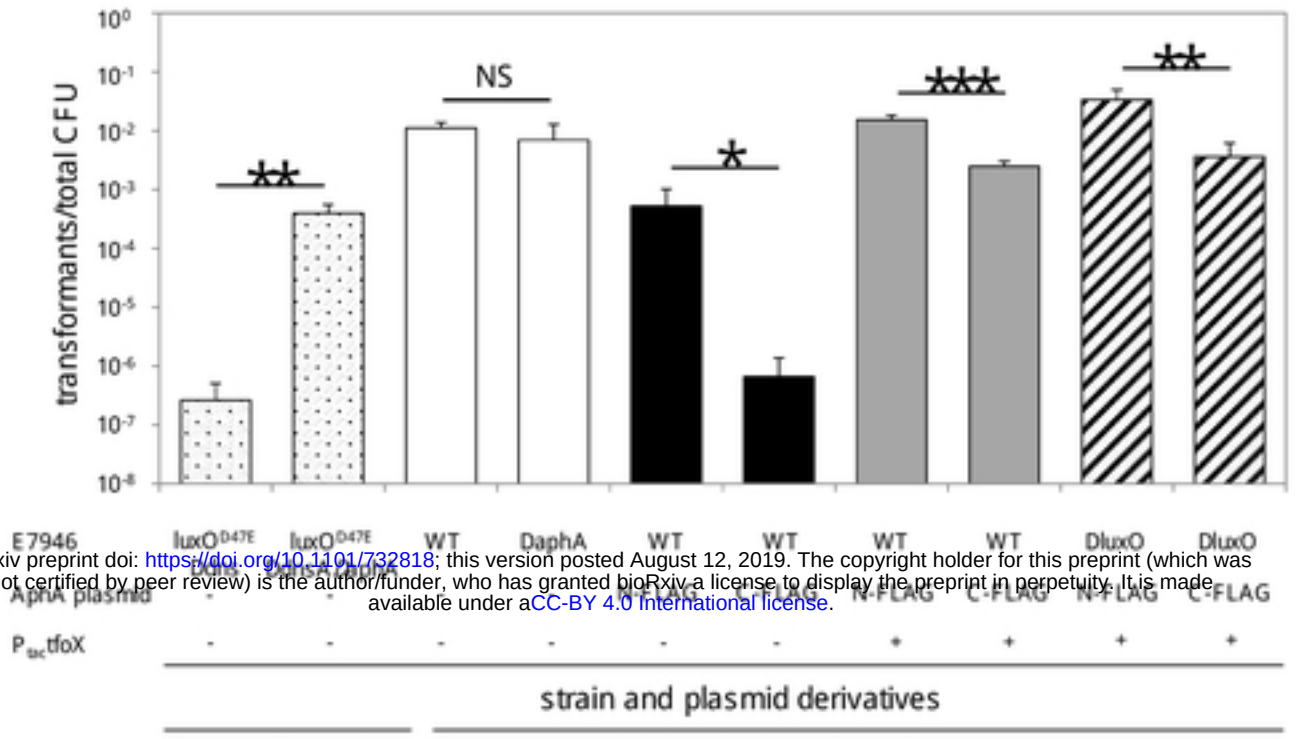

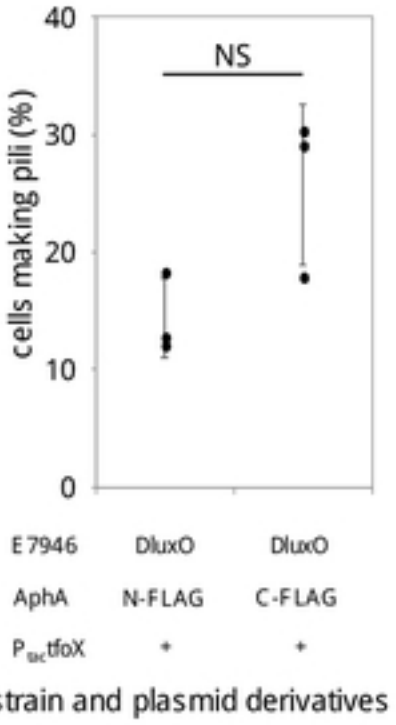

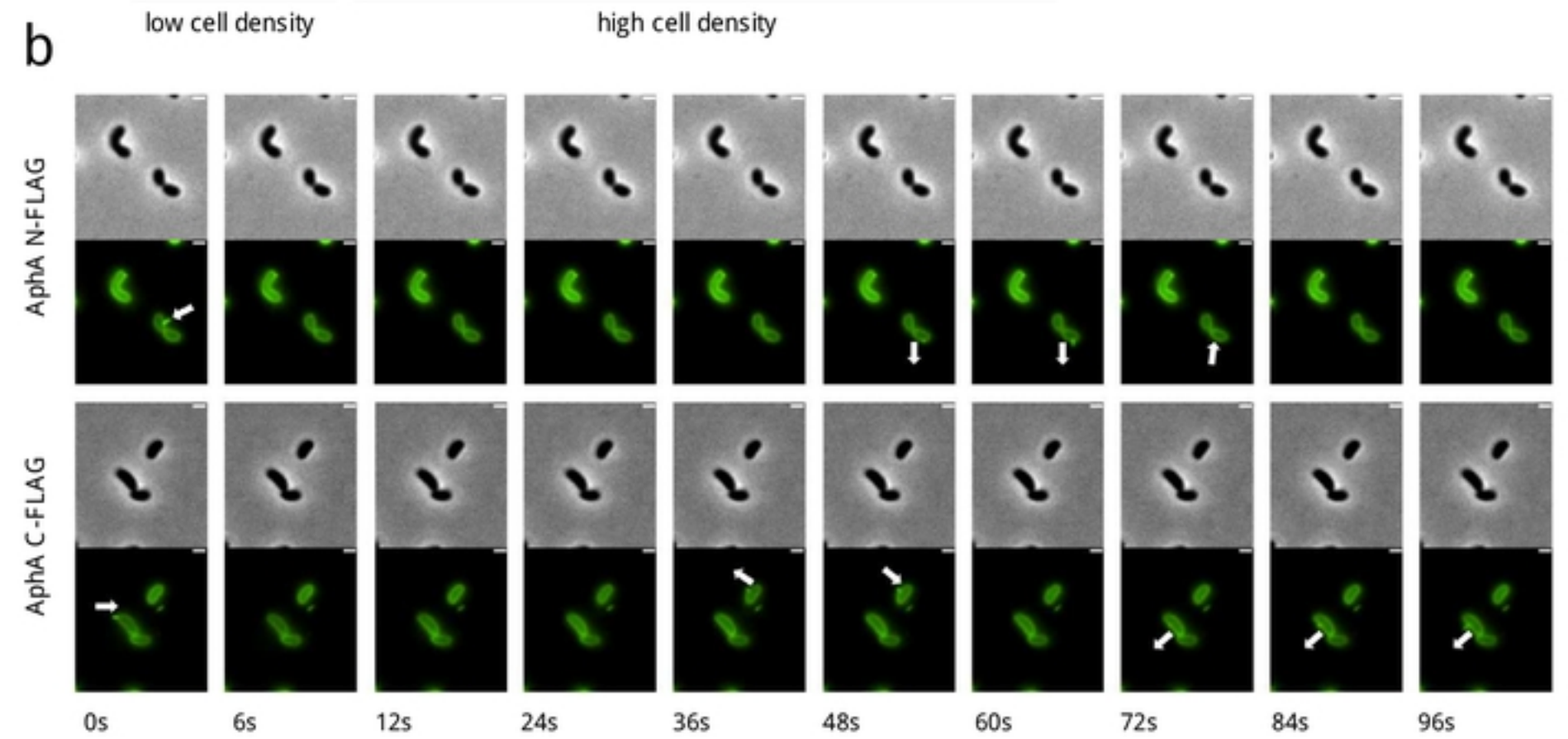

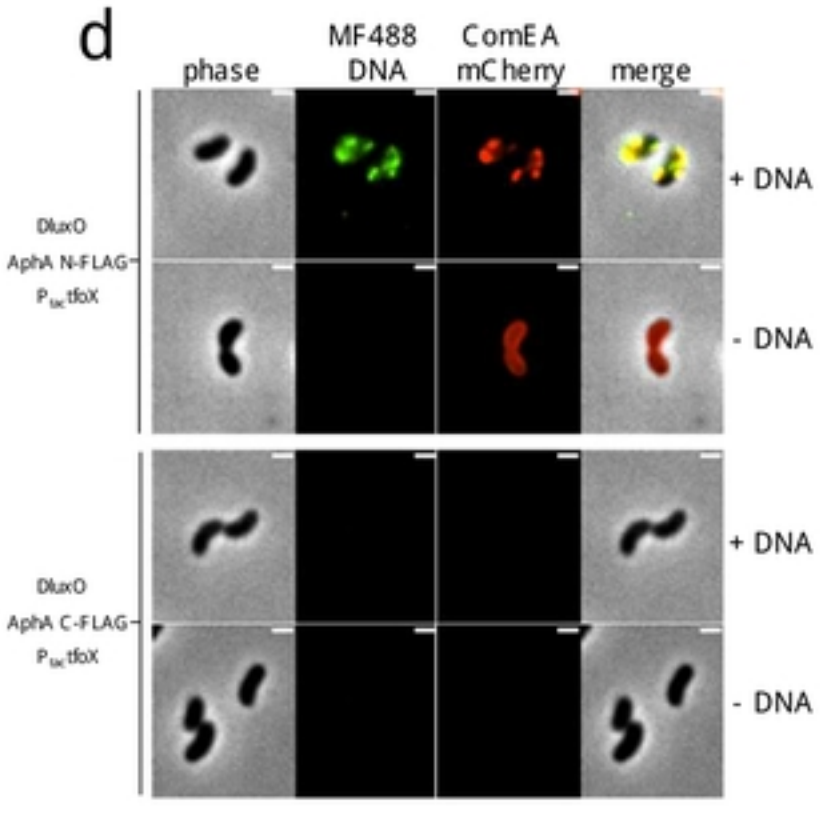

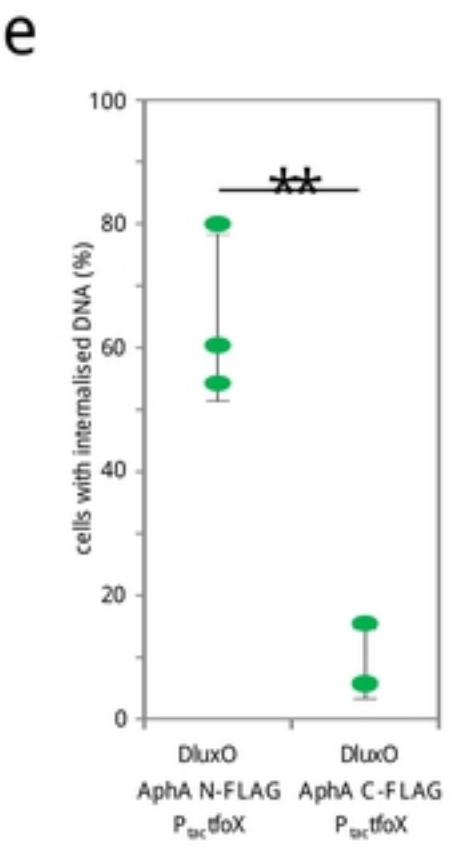

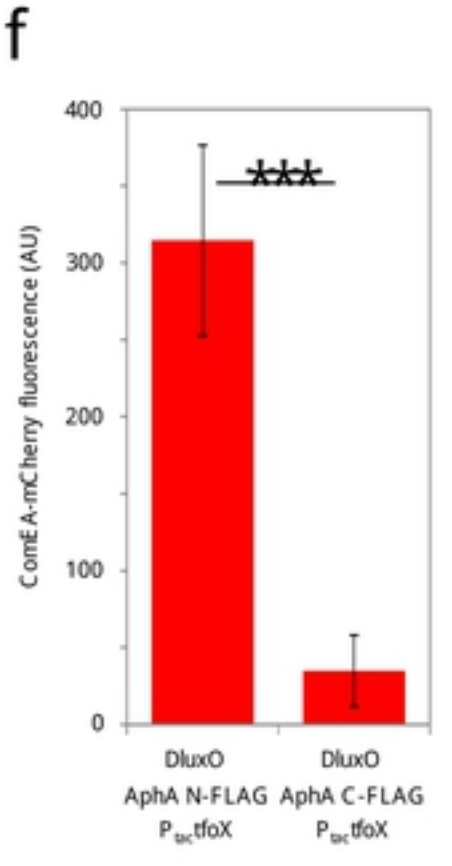

Figure 6